Final Report

Probabilistic Finite Elements for Fatigue and Fracture Analysis

by

Ted Belytschko and Wing Kam Liu

Northwestern University
Department of Mechancial Engineering
Evanston Illinois 60208

NASA Grant Number: NAG3-822

NASA Project Manager: Dr. Christos C. Chamis

Publications sponsored by **NASA Grant NAG3-822**
"Probabilistic Finite Elements for Fatigue and Fracture Analysis,"
February 1, 1988 to March 31, 1991. ($252,029).

1) "Probabilistic Finite Element Methods," *Computational Mechanics of Probabilistic and Reliability Analysis*, ELMEPRESS International, pp. 325-342, 1989.

2) "Brittle Fracture Reliability by Probabilistic Finite Elements," (with G. H. Besterfield, M. A. Lawrence and T. Belytschko), *Computational Mechanics of Probabilistic and Reliability Analysis,* ELMEPRESS International, pp. 343-370, 1989.

3) "Brittle Fracture Reliability by Probabilistic Finite Elements," (with G. H. Besterfield, M. A. Lawrence and T. Belytschko), *Journal of Engineering Mechanics*, ASCE, Vol. 116 (3), pp. 642-659, 1990.

4) "Fatigue Crack Growth Reliability," (with M. A. Lawrence, G. H. Besterfield and T. Belytschko), *Journal of Engineering Mechanics*, ASCE, Vol. 116 (3), pp. 698-708, 1990.

5) "A Variationaly Coupled FE-BE Method for Elastically and Fracture Mechanics," (with Lu, Y.Y., and Belytschko, T.) *Computer Methods in Applied Mechanics and Engineering,* Vol 85, pp. 21-37, 1991.

6) "Fatigue Crack Growth Reliability by Probabilistic Finite Elements," (with Besterfield, G. H.,Lawrence, M. A., and Belytschko, T. B.) *Computer Methods in Applied Mechanics and Engineering*, vol. 86, pp.297-320, 1991.

7) "A Stochastic Damage Model for the Rupture Prediction of a Multi-Phase Solid: Part I: Parametric Studies", (With Lua, Y.J. and Belytschko, T.) *Int. J. Fracture Mech.*, 55, pp.321-340, 1992.

8) "A Stochastic Damage Model for the Rupture Prediction of a Multi-Phase Solid: Part II: Statistical Approach", (With Lua, Y. J., Liu and Belytschko, T.), *Int. J. Fracture Mech.*, 55, pp.341-361, 1992.

9) "Finite Element Reliability Analysis of Fatigue Life," (with H. H. Harkness, and T. Belytschko) *Nuclear Engineering and Design*, 113, pp.209-224, 1992.

10) "Stochastic Computational Mechanics in Brittle Fracture and Fatigue," (with Y. J. Lua and T. Belytschko) *Nonlinear Stochastic Mechanics*, N. Bellomo and F. Casciati, Editors, IUTAM Symposium Turin, Springer-Verlag Berlin Heidlberg, 1992, PP. 355-366.

11) "Stochastic Computational Mechanics for Aerospace Structures," (With Lua, Y. J. and Belytschko, T.) *Computational Nonlinear Mechanics in Aerospace Engineering,* S. N. Atluri ed. (1992), in press

12) "A Stochastic Approach to the Fatigue Growth Reliability," *Probabilistic Mechanics and Structural and Geotechnical Reliability,* Y. K. Lin, editor, ASCE, Denver, Colorado, July 8-10, 1992, pp. 324-327.

13) "Stochastic Computational Mechanics for Aerospace Structures," (With Lua, Y. J. and Belytschko, T.) *Computational Nonlinear Mechanics in Aerospace Engineering*, S. N. Atluri ed. (1992), in press

14) "Probabilistic Finite Element Methods" (with Y. J. Lua, and T. Belytschko), to appear in *Probabilistic Structural Mechanics Handbook* , C. Sundararajan, ed., 1992.

15) "Life Predication of a Curvilinear Fatigue Crack Growth by SBEM," ASME 1992 Annual Winter Symposium on *Reiability for Mechanical System Design*.

Books

"Computational Mechanics of Probabilistic Reliability Analysis," eds. W. K. Liu and T. Belytschko, ELMEPRESS International, 1989, 622 pp.

1. INTRODUCTION

It is becoming increasingly evident that traditional and especially deterministic methods will not be sufficient to properly design advanced structures or structural components subjected to a variety of complex, and cyclic loading conditions. Due to uncertainty in loading conditions, material behavior, geometric configuration, and supports, the stochastic computational mechanics, which accounts for all these uncertain aspects, has to be applied to provide rational reliability analysis and to describe the behavior of the structure. The fundamentals of stochastic computational mechanics and its application to the analysis of uncertain structural systems are summarized and recapitulated in the book (Liu and Belytschko, 1989).

While the theory of statistics and structural reliability has been used successfully in modeling the uncertain nature of structures, load environments, and in computing the probability of failure, its application is only limited in simple structures with linear constitutive behavior. Due to the complexity in the geometry, external loads, and nonlinear material behavior, more advanced computational tools such as Finite Element Methods (FEMs) or Boundary Integral Equation Methods (BIEMs), have to be employed to provide the necessary computational framework for analyzing structural response. The combination of these advanced computational tools with the theory of statistics and structural reliability has become a rational way for the safety assessment and uncertainty characterization of complex structures. In this Chapter, attenuation is focused on the development of Probabilistic Finite Element Method (PFEM), which combines the finite element method with statistics and reliability methods, and its application to linear, nonlinear structural mechanics problems and fracture mechanics problems. The novel computational tool based on the Stochastic Boundary Element Method is also given for the reliability analysis of a curvilinear fatigue crack growth.

The existing PFEMs have been applied to solve for two types of problems: (1) determination of the response uncertainty in terms of the means, variance and correlation coefficients; (2) determination the probability of failure associated with prescribed limit states. While the second order statistic moments of a response are not sufficient for a complete reliability analysis, these moments offer useful statistical information and serve as a measures of reliability. Furthermore, due to the lack of multivariate distribution function of random variables, a meaningful risk assessment and failure analysis may not be feasible.

The perturbation method has been used extensively in developing PFEM due to its simplicity and versatility. Cambou (1975) appears to have been the first to apply the first order perturbation method for the finite element solution of linear static problems with loading and system stochasticity. Baecher and Ingra (1981) also used the same techniques for settlements predictions. The perturbation method in conjunction with finite element method has also been adopted by Handa and Anderson (1981) for static problems of beam and frame structures, by Ishii and Suzuki (1987) for slope stability reliability analysis, and by Righetti and Harrop-Williams (1988) for static stress analysis for soils. The accuracy, convergence and computational efficiency of the perturbation method have been compared with those from Neumann expansion method and direct Monte Carlo Simulation (MCS) method (Shinozuka and Yamazaki, 1988; Shinozuka and Deodatis, 1988). The PFEM based on the second-order perturbation approximation has been introduced by Hisada and Nakagiri (1981 and 1985) for static problems and for eigenvalue problems.

Extensive research on the PFEM has been developed by the authors and their colleagues at Northwestern University in the recent years. The PFEM based on the second-order perturbation has been developed to estimate the statistic moments of the response for linear static problems (Liu et al.,

1986a), nonlinear dynamic problems (Liu et al., 1986b), and inelastic problems (Liu et al., 1987). The formulation based on the single-field variational principle has been extended by Liu et al. (1988a) to the three-field Hu-Washizu variational principle formulation, which has far greater versatility. The numerical instability resulting from the secular terms in the perturbation has been removed by Liu et al. (1988b) based on Fourrier analysis. The perturbation methods have been shown to provide efficient and accurate results for small random fluctuations in the random parameters. An extensive review on the application of perturbation methods in developing PFEM has been given by Benaroya and Rehak (1988).

The finite element method coupled with the First and Second-Order Reliability Methods (FORM and SORM) has been developed by Der Kiureghian and Ke (1985, 1988) for linear structural problems and Liu and Der Kiureghian (1991) for geometrically non-linear problems. The most critical step in this method is the development of an efficient search algorithm for locating the point at which the response surface is to be expanded in a first or second order Taylor series. This point is obtained by an iterative optimization algorithm, which involves repeated computation of the limit state function and response derivatives. Unlike the method of direct differentiation (Der Kiureghian and Ke, 1988; Liu and Der Kiureghian, 1991; Zhang and Der Kiureghian, 1991), the PFEM based on the perturbation approximation in conjunction with FORM has been developed by Besterfield et al (1990, 1991) for the reliability analysis of brittle fracture and fatigue. In a slightly different context, the PFEM has been developed by Faravelli (1986, 1989) that couples response surface approach with deterministic finite element formulation. The finite element simulation coupled with the polynomial response surface fitting has been also proposed by Grigoriu (1982). Using a deterministic finite element code and finite differences, an advanced algorithm based on the Fast Probability Integration (FPI) has been developed by Wu et al (1990) to generate the entire part of the Cumulative Distribution Function (CDF) of the response. The performance of the FPI based on either advanced mean-value method or advanced mean value first-order method has been demonstrated by Cruse et al. (1988) through the reliability analysis of turbine blade.

In addition to the PFEM, the Stochastic Boundary Element Method (SBEM) has been developed and adopted recently by researchers. The SBEM that combines the deterministic boundary element method with perturbation expansions has been developed by Ettouney et al. (1989) and Dasgupta (1992) for the determination of the statistic moments of both displacements and tractions. Most recently, the authors have developed the SBEM, which combines the mixed boundary integral equation method (Lua et al., 1992c) with FORM, for the study of probabilistic fatigue crack growth (Lua et al., 1992d).

This Chapter presents an overview of the PFEM developed by the authors and their colleagues in the recent years. The primary focus is placed on the development of PFEM for both structural mechanics problems and fracture mechanics problems. The perturbation techniques are used as major tools for the analytical derivation. The remainder of this Chapter is organized as follows. In Section 2, the representation and discretization of random fields are presented. The development of PFEM for the general linear transient problem and nonlinear elasticity using Hu-Washizu variational principle are given in Section 3, and 4, respectively. The computational aspects are discussed in Section 5. The application of PFEM to the reliability analysis of both brittle fracture and fatigue is given in Section 6. A novel stochastic computational tool based on SBEM is presented in Section 7. The final conclusions are drawn in Section 8.

2. RANDOM FIELD DISCRETIZATION

2.1 Background

The randomness of a stochastic system can be described in three forms, random variables, random process in space, and random process in time. The random process in space is also called

random field. The aspects of random fields and its application to engineering problems are given by Vanmarcke (1984). Various methods have been used to the numerical representation of random processes. The statistical characterization for thunderstorm winds has been given by Twisdale and Dunn (1983) and Twisdale and Vickery (1991). The spectral representation of random processes based on computer simulation has been proposed by Shinozuka (1987).

The spatial variability of mechanical properties of a system and the intensity of a distributed load can conveniently be represented by means of random fields. Due to the discrete nature of the finite element formulation, the random field must also be discretized into random variables. This process is commonly known as random field discretization. Various methods have been developed in the representation of random fields. They are: the midpoint method (Hisada and Nakagiri, 1985; Der Kiureghian and Ke, 1988; Yamazaki et al., 1988), the spatial averaging method (Vanmarcke and Grigoriu, 1983), and series expansion method (Lawrence, 1987; Spanos and Ghanem, 1988). In this section, the interpolation method (Liu et al., 1986a) is described. In this method, the random field is represented by a set of deterministic shape functions and the random nodal values of the field. The size of the random field element is controlled by the correlation length of the field and the stability of the probability transformation used in the reliability methods (FORM and SORM). The random field mesh should be so fine to capture the fluctuation of the random field. On the other hand, the random field mesh should not be so small that high correlated stochastic variables of adjacent elements cause numerical instability in the probability transformation, which is required in the reliability methods (FORM and SORM). As suggested by Der Kiureghian (1985), two separate meshes for the finite element and for random fields have to be used in the numerical implementation.

Since the computational effect in the determination of response derivatives or sensitivities is proportional to the number of random variables, it is desirable to use as few random variables as possible to represent a random field. To achieve this goal, the transformation of the original random variables into a set of uncorrelated random variables has been introduced by Liu et al. (1986a) through an eigenvalue orthogonalization procedure. Comparison with a Monte-Carlo simulation demonstrates that a few of these uncorrelated variables with larger eigenvalues are sufficient for the accurate representation of the random field. This technique along with other computational aspects is presented in Section 5.

2.2 Interpolation Method

Let $b(\mathbf{x})$ represent the random field. In PFEM, $b(\mathbf{x})$ is approximated by

$$b(\mathbf{x}) = \sum_{i=1}^{q} N_i(\mathbf{x})\, b_i \tag{2-1}$$

where $N_i(\mathbf{x})$ represent the shape functions and b_i the discretized values of $b(\mathbf{x})$ at x_i, $i = 1, \ldots, q$. It follows from Eq. (2-1) that

$$db(\mathbf{x}) = \sum_{i=1}^{q} N_i(\mathbf{x})\, db_i \tag{2-2}$$

and

$$db^2(\mathbf{x}) = \sum_{i\,j=1}^{q} N_i(\mathbf{x})\, N_j(\mathbf{x})\, db_i\, db_j \tag{2-3}$$

where

$$db_i = b_i - \bar{b}_i \tag{2-4}$$

and $\bar{b}_i$ represent the mean values of b_i (also denoted by the expectation operator E[.]). From Eq. (2-1) the expectation and the covariance of b(**x**) are, by definition,

$$E[b(\mathbf{x})] = \int_{-\infty}^{+\infty} b(\mathbf{x})\, f(\mathbf{b})\, d\mathbf{b} \tag{2-5}$$

$$= \sum_{i=1}^{q} N_i(\mathbf{x})\, E[b_i] \tag{2-6}$$

and

$$Cov[b(\mathbf{x}_k), b(\mathbf{x}_m)] = \int_{-\infty}^{+\infty} [b(\mathbf{x}_k) - \bar{b}(\mathbf{x}_k)]\, [b(\mathbf{x}_m) - \bar{b}(\mathbf{x}_m)]\, f(\mathbf{b})\, d\mathbf{b} \tag{2-7}$$

$$= \sum_{i\,j=1}^{q} N_i(\mathbf{x}_k)\, N_j(\mathbf{x}_m)\, Cov(b_i, b_j) \tag{2-8}$$

respectively, where f(**b**) is the multivariate probability density function; $\mathbf{x}_k$ and $\mathbf{x}_m$ are any two points in the domain of **x**.

From second-moment analysis, the mean of any function S[b(**x**),**x**] at any point $\mathbf{x}_k$ and the covariance of the function between any two points $\mathbf{x}_k$ and $\mathbf{x}_m$ can be written as

$$E[S_k] \approx \bar{S}_k + \frac{1}{2} \sum_{i\,j=1}^{q} \frac{\partial^2 \bar{S}_k}{\partial b_i \partial b_j} Cov(b_i, b_j) \tag{2-9}$$

and

$$\mathrm{Cov}[S_k, S_m] \approx \sum_{i\,j=1}^{q} \left(\frac{\partial \bar{S}_k}{\partial b_i}\right)\left(\frac{\partial \bar{S}_m}{\partial b_j}\right) \mathrm{Cov}(b_i, b_j) \tag{2-10}$$

where

$$S_k = S[b(\mathbf{x}), \mathbf{x}_k] \tag{2-11}$$

and the superposed bar implies evaluation at $\bar{\mathbf{b}}$. The error in Eqs. (2-9) and (2-10) arises from: (i) the truncation of higher order moments and (ii) the discretization of the random field $b(\mathbf{x})$ by the finite vector $\mathbf{b}$. If the randomness in $b(\mathbf{x})$ is small, then the first error will be small for a smooth function and the second-moment analysis is applicable. The error due to discretization in Eqs. (2-6) and (2-8) has been studied by Liu et al. (1987) .

When the random field discretization is coupled with a FEM discretization, as in PFEM, q need not be equal to the number of finite elements NUMEL and the shape function $N_j(\mathbf{x})$ need not be the same as the finite element interpolants for the displacement field. As indicated before, two meshes, one depending on structural topology, the other on correlation length can be employed to improve the computational efficiency.

3. PROBABILISTIC FINITE ELEMENTS FOR LINEAR PROBLEMS

The probabilistic finite element method (PFEM) is used to study of systems with parametric uncertainties in both the unknown function and mathematical operators acting on it. The loads can be either deterministic or random. In this section, the second-order perturbation is employed to develop PFEM for a general linear transient problem. By applying the second-order perturbation, the random linear system equations can be replaced by a finite number of identical deterministic system equations up to second-order. The effective load in each of these equations depends on the randomness of the system and the solutions of the all the lower order equations.

Due to the space limitation, the review on the deterministic finite element method is not given here. The state-of-the-art of finite element techniques can be found in the review article by Noor (1991). Using either the single field variational principle or Galerkin formulation, the discretized linear equations of motion are

$$\mathbf{M}\,\mathbf{a}(\mathbf{b}, t) + \mathbf{K}(\mathbf{b})\,\mathbf{d}(\mathbf{b}, t) = \mathbf{f}(\mathbf{b}, t) \tag{3-1}$$

where $\mathbf{M}$ and $\mathbf{K}(\mathbf{b})$ are the (neq × neq) global mass and stiffness matrices, respectively; $\mathbf{a}(\mathbf{b}, t)$, $\mathbf{d}(\mathbf{b}, t)$, and $\mathbf{f}(\mathbf{b}, t)$ are the (neq × 1) nodal acceleration, displacement, and force vectors, respectively; neq is the number of equations; and $\mathbf{b}$ is a q-dimensional discretized random variable vector, i.e., $b_i = b(\mathbf{x}_i)$, where $\mathbf{x}_i$ is the spatial coordinate vector. The mass is usually assumed to be deterministic whereas the probabilistic distributions for the stiffness and external force are represented by a generalized covariance matrix, $\mathrm{Cov}(b_i, b_j)$, i, j = 1, ..., q. It is worth noting that the stiffness matrix can be expressed in terms of the generalized gradient matrix, $\mathbf{B}(\mathbf{x})$, and the material response matrix, $\mathbf{D}(\mathbf{b}, \mathbf{x})$. In this formulation, the random vector, $\mathbf{b}$, can represent a

random material property (e.g., Young's modulus) and/or a random load.

The application of second-moment analysis to develop PFEM involves expanding all random functions about the mean value of the random vector **b**, denoted by $\bar{\mathbf{b}}$, via Taylor series and retaining only terms up to second-order terms. That is, for a small parameter, ξ, the random displacement function **d**(**b**, t) is expanded about $\bar{\mathbf{b}}$ via a second-order perturbation as follows:

$$\mathbf{d}(\mathbf{b}, t) = \bar{\mathbf{d}}(t) + \xi \sum_{i=1}^{q} \bar{\mathbf{d}}_{b_i}(t)\,\Delta b_i + \frac{1}{2}\xi^2 \sum_{i}\sum_{j=1}^{q} \bar{\mathbf{d}}_{b_i b_j}(t)\,\Delta b_i \Delta b_j \tag{3-2}$$

where $\bar{\mathbf{d}}(t)$, $\bar{\mathbf{d}}_{b_i}(t)$, and $\bar{\mathbf{d}}_{b_i b_j}(t)$ represent the mean displacement, the first-order variation of displacement with respect to b_i evaluated at $\bar{\mathbf{b}}$, and the second-order variation of displacement with respect to b_i and b_j evaluated at $\bar{\mathbf{b}}$, respectively and Δb_i represents the first-order variation of b_i about $\bar{b}_i$. In a similar manner, **K**(**b**), **a**(**b**, t), and **f**(**b**, t) are also expanded about $\bar{b}_i$ via a second-order perturbation. Substitution of the second-order perturbations of the random function **d**(**b**, t), **K**(**b**), **a**(**b**, t) and **f**(**b**, t) into (3-1) and collecting terms of order 1, ξ, and ξ^2 yields the following equations:

Zeroth-Order Equations

$$\mathbf{M}\,\bar{\mathbf{a}}(t) + \bar{\mathbf{K}}\,\bar{\mathbf{d}}(t) = \bar{\mathbf{f}}(t) \tag{3-3}$$

First-Order Equations (for each Δb_i, i = 1, ..., q)

$$\mathbf{M}\,\bar{\mathbf{a}}_{b_i}(t) + \bar{\mathbf{K}}\,\bar{\mathbf{d}}_{b_i}(t) = \bar{\mathbf{F}}_{b_i}(\bar{\mathbf{d}}, t) \tag{3-4}$$

where

$$\bar{\mathbf{F}}_{b_i}(\bar{\mathbf{d}}, t) = \bar{\mathbf{f}}_{b_i}(t) - \bar{\mathbf{K}}_{b_i}\,\bar{\mathbf{d}}(t) \tag{3-5}$$

Second-Order Equations (i and j are summed from 1 to q)

$$\mathbf{M}\,\bar{\mathbf{a}}_2(t) + \bar{\mathbf{K}}\,\bar{\mathbf{d}}_2(t) = \bar{\mathbf{F}}_2(\bar{\mathbf{d}}, t) \tag{3-6}$$

where

$$\bar{\mathbf{F}}_2(\bar{\mathbf{d}}, t) = \sum_{i\,j=1}^{q} \{ \tfrac{1}{2}\bar{\mathbf{f}}_{b_i b_j}(t) - \tfrac{1}{2}\bar{\mathbf{K}}_{b_i b_j}\bar{\mathbf{d}}(t) - \bar{\mathbf{K}}_{b_i}\bar{\mathbf{d}}_{b_j}(t)\} \mathrm{Cov}(b_i, b_j) \tag{3-7}$$

$$\bar{\mathbf{a}}_2(t) = \tfrac{1}{2}\sum_{i\,j=1}^{q} \bar{\mathbf{a}}_{b_i b_j}(t)\,\mathrm{Cov}(b_i, b_j) \tag{3-8}$$

$$\bar{\mathbf{d}}_2(t) = \tfrac{1}{2}\sum_{i\,j=1}^{q} \bar{\mathbf{d}}_{b_i b_j}(t)\,\mathrm{Cov}(b_i, b_j) \tag{3-9}$$

The solution process for Eqs. (3-3) through (3-9) can be performed in parallel since only one effective stiffness matrix needs to be formed. Therefore, the total solution requires one factorization of the effective stiffness matrix and q+2 forward reductions and back substitutions of an (neq × neq) system of linear equations to obtain the zeroth-, first-, and second-order solutions.

To illustrate the performance of PFEM, a simple two degree of freedom spring-mass system is presented here. The computed results are compared with those obtained using (1) Monte Carlo Simulation (MCS) and (2) Hermite-Gauss Quadrature (HGQ) schemes. The problem is depicted in Fig. 7-1. A sinusoidal vector forcing function is used:

$$F(t) = \begin{bmatrix} 0.0 \\ 25.0 \times 10^6 \sin 2000\, t \end{bmatrix} \tag{3-10}$$

The random spring constants K_1 and K_2 are normally distributed with a coefficient of variation (i.e. σ/μ) equal to 0.05. The mean spring constants are 24×10^6 and 12×10^6, respectively. The deterministic masses m_1 and m_2 are 0.372 and 0.248, respectively. A stiffness-proportional damping of 3% is included. The probabilistic equations derived earlier are solved by the implicit Newmark-β method (Ma, 1986). The mean amplitude $\overline{d_1}$ is depicted in Fig. 7-2 for all the three numerical methods-PFEM, HGQ and MCS. The PFEM solution compares very well with the other two methods. For the variance of d_1 the PFEM solution, plotted in Fig. 7-3, seems to overshoot the variance at large time. The $\pm 3\sigma$ bounds for the displacement d_1 is plotted in Fig. 7-4.

4. PROBABILISTIC FINITE ELEMENTS FOR NON-LINEAR PROBLEMS

The probabilistic finite element method has been developed in the previous section using the single-filed variational principle. Due to the direct stiffness matrix approach used, it can be only applied to solve a limited number of problems with uncertainty in loading and material properties.

In order to consistently handle problems with randomness in the equilibrium equations, domain, and boundary conditions, the three-field Hu-Washizu variational principle will be employed to develop PFEM. An additional advantage of using the Hu-Washizu variational principle involves the elimination of the locking phenomena (Belytschko and Bachrach, 1986) and suppression of hourglass modes (Belytschko et al., 1984). Solution of three stationary conditions for the compatibility relation, constitutive law, and equilibrium yield the variations in displacement, strain and stress. The statistics such as expectation, autocovariance, and correlation of displacement, strain and stress are then determined.

Using matrix notation, the Hu-Washizu Variational Principle (HWVP) for nonlinear problems adopted in this Section is (see Liu et al., 1988c)

$$\int_{\Omega} \delta\varepsilon^{T} (\psi - \sigma)\, d\Omega - \int_{\Omega} \delta\sigma^{T} (\varepsilon - \nabla \mathbf{u})\, d\Omega$$

$$+ \int_{\Omega} \delta(\nabla \mathbf{u})^{T} \sigma\, d\Omega - \int_{\Omega} \delta\mathbf{u}^{T} \mathbf{F}\, d\Omega - \int_{\partial\Omega_h} \delta\mathbf{u}^{T} \mathbf{h}\, d\Gamma = 0 \qquad (4\text{-}1)$$

where ε, σ, and $\mathbf{u}$ are independent random field variables representing the nonsymmetric measure of the strain, first Piola-Kirchhoff stress, and displacement, respectively; ψ is a nonlinear function of the deformation gradient; and a superscript T represents the transpose. In Eq. (4-1): Ω, $\partial\Omega_h$, $\mathbf{F}$, $\mathbf{h}$, and $\nabla\mathbf{u}$ represent the domain, traction boundary, body force vector, prescribed traction vector, and the nonsymmetric part of the displacement gradient, respectively; δ represents a virtual quantity. The surface and volume integrals in Eq. (4-1) can be expressed via parametric representation:

$$d\Gamma = J_s\, dA \qquad \text{and} \qquad d\Omega = J_v\, dR \qquad (4\text{-}2)$$

respectively, where J_s and J_v represent the surface and volume Jacobians, respectively; and R and A represent the reference domain and boundary, respectively. Random domains and boundaries are incorporated into the formulation through randomness in the gradient operator and Jacobians. The application of second-order perturbation techniques in the HWVP involves the expansion of all random functions about the mean value of the random field $b(\mathbf{x})$ denoted by $\bar{b}(\mathbf{x})$ and retaining only up to second-order terms, i.e., for a given small parameter [ξ = the scale of randomness in $b(\mathbf{x})$], the random function ψ is expanded about $\bar{b}$ at a given point $\mathbf{x}$ in the reference domain as follows:

$$\psi \approx \psi^{0} + \xi (\psi' + C^{0}\varepsilon') + \xi^{2} (\psi'' + C'\varepsilon' + C^{0}\varepsilon'') \qquad (4\text{-}3)$$

where the superscripts nought, prime, and double prime represent the random functions evaluated at $\bar{b}$, the first-order variation due to variations in $\bar{b}$, and the second-order variation, respectively. The first elasticity tensor, $\mathbf{C}$ in Eq. (4-3) is given by

$$C_{ijkm} = \frac{\partial^2 W}{\partial G_{ij} \partial G_{km}} \tag{4-4}$$

where W is the strain energy density function; and $\mathbf{G}$ is the deformation gradient. Similarly, the rest of random functions ε, σ, $\mathbf{F}$, $\mathbf{h}$, J_S, J_V, $\nabla\mathbf{u}$ and $\delta(\nabla\mathbf{u})^T$ can also be expressed as second order perturbations (see Liu et al., 1988a). After substituting the second order perturbations of all these random functions into Eq.(4-1), the following three equations for the zeroth-, first-, and second-order nonlinear PHWVP are obtained:

Zeroth-Order Variational Principle

$$\int_R \delta\varepsilon^T (\psi^0 - \sigma^0)\, J_v^0\, dR - \int_R \delta\sigma^T (\varepsilon^0 - \nabla^0 \mathbf{u}^0)\, J_v^0\, dR$$

$$+ \int_R \delta(\nabla^0 \mathbf{u})^T \sigma^0\, J_v^0\, dR - \int_R \delta\mathbf{u}^T \mathbf{F}^0\, J_v^0\, dR - \int_{\partial R_h} \delta\mathbf{u}^T \mathbf{h}^0\, J_s^0\, dA = 0 \tag{4-5}$$

First-Order Variational Principle (ξ terms)

$$\int_R \delta\varepsilon^T [(\mathbf{C}^0\varepsilon' - \sigma')\, J_v^0 + \psi'\, J_v^0 + (\psi^0 - \sigma^0)\, J_v'] \, dR$$

$$- \int_R \delta\sigma^T [(\varepsilon' - \nabla^0 \mathbf{u}' - \nabla' \mathbf{u}^0)\, J_v^0 + (\varepsilon^0 - \nabla^0 \mathbf{u}^0)\, J_v'] \, dR$$

$$+ \int_R \{[\delta(\nabla^0 \mathbf{u})^T \sigma' + \delta(\nabla' \mathbf{u})^T \sigma^0]\, J_v^0 + \delta(\nabla^0 \mathbf{u})^T \sigma^0\, J_v'\} \, dR$$

$$- \int_R \delta\mathbf{u}^T (\mathbf{F}'\, J_v^0 + \mathbf{F}^0\, J_v')\, dR - \int_{\partial R_h} \delta\mathbf{u}^T (\mathbf{h}'\, J_s^0 + \mathbf{h}^0\, J_s')\, dA = 0 \tag{4-6}$$

Second-Order Variational Principle (ξ^2 terms)

$$\int_R \delta\varepsilon^T [(\mathbf{C}^0\varepsilon'' - \sigma'')\, J_v^0 + (\mathbf{C}\varepsilon'\varepsilon' + \psi'')\, J_v^0 + (\mathbf{C}^0\varepsilon' + \psi' - \sigma')\, J_v' + (\psi^0 - \sigma^0)\, J_v''] \, dR$$

$$- \int_R \delta\sigma^T [(\varepsilon'' - \nabla^0 \mathbf{u}'' - \nabla' \mathbf{u}' - \nabla'' \mathbf{u}^0) J_v^0 + (\varepsilon' - \nabla^0 \mathbf{u}' - \nabla' \mathbf{u}^0) J_v' + (\varepsilon^0 - \nabla^0 \mathbf{u}^0) J_v''] \, dR$$

$$+ \int_R \{ [\delta(\nabla^0 \mathbf{u})^T \sigma'' + \delta(\nabla' \mathbf{u})^T \sigma' + \delta(\nabla'' \mathbf{u})^T \sigma^0] J_v^0$$

$$+ [\delta(\nabla^0 \mathbf{u})^T \sigma' + \delta(\nabla' \mathbf{u})^T \sigma^0] J_v' + \delta(\nabla^0 \mathbf{u})^T \sigma^0 J_v'' \} \, dR$$

$$- \int_R \delta\mathbf{u}^T (\mathbf{F}'' J_v^0 + \mathbf{F}' J_v' + \mathbf{F}^0 J_v'') \, dR$$

$$- \int_{\partial R_h} \delta\mathbf{u}^T (\mathbf{h}'' J_s^0 + \mathbf{h}' J_s' + \mathbf{h}^0 J_s'') \, dA = 0 \tag{4-7}$$

It should be noted that all random functions with the superscript (") or (') in Eqs. (4-6)-(4-7) are, in general, described through spatial expectation and autocovariance functions. Therefore, in addition to the usual finite element approximation of the displacement field, the random fields are also discretized with q shape functions. To be consistent with the finite element approximation and to maintain the accuracy of the discretized random field [i.e., b(**x**)], the random functions ψ, **C**, **F**, **h**, J_s, and J_v, which are, in general, functions of b(**x**) and **x**, are first discretized with the same q shape functions as the random fields. For example, the finite element approximation of **C** is given by

$$\mathbf{C} \approx \mathbf{C}^0 + \xi \mathbf{C}' + \xi^2 \mathbf{C}'' \tag{4-8}$$

or

$$\mathbf{C} \approx \sum_{I=1}^{q} \phi_I(\mathbf{x})(\mathbf{C}_I^0 + \xi \mathbf{C}_I' + \xi^2 \mathbf{C}_I'') \tag{4-9}$$

where; $\phi_I(\mathbf{x})$ are the q shape functions; $\mathbf{C}_I^0$ denotes the Ith nodal value of **C** evaluated at $\bar{b}$; $\mathbf{C}_I'$ denotes the first-order variation of $\mathbf{C}(\mathbf{x}_I, \bar{b})$ due to variations Δb_i; and $\mathbf{C}_I''$ denotes the second-order variation. The last two are then expanded in terms of the random variables b_i and given by

$$\mathbf{C}_I' = \sum_{i=1}^{q} (\mathbf{C}_I')_i \, \Delta b_i \tag{4-10}$$

and

$$C_I'' = \frac{1}{2} \sum_{i\,j=1}^{q} (C_I'')_{ij}\, \Delta b_i\, \Delta b_j \tag{4-11}$$

respectively. The factor 1/2 is included in order to be consistent with the second-order Taylor series expansion. The nodal values $(C_I')_i$ and $(C_I'')_{ij}$ can be obtained by partial differentiation of C or by a least-square fit to the actual data. Similar definitions can be developed for the rest of random functions (see Liu et al., 1988a).

Substituting the given approximation of all random functions into the zero-order, first-order, and second-order PHWVPs (Eqs. (4-5)-(4-7)), and using the three stationary conditions (strain-displacement, stress-strain, and equilibrium), the zeroth, first and second order equations can be obtained (see Liu et al., 1988a). The zeroth-order equations require an iterative solution technique, but the first-order and second-order equation are linear. After determining the zeroth-, first-, and second- order solutions, the expectations and autocovariance matrices for the displacements, strains, and stresses can be obtained.

The applicability and effectiveness of the PFEM for nonlinear problems was demonstrated by Liu et al. (1988a) through the problem of a cantilever beam subjected to large deflection. The Saint Venant-Kirchhoff model for nonlinear elasticity with randomness in the external force, beam height, and material properties were considered. The probabilistic distribution for displacement, strain and stress were also presented.

To reduce computational effort, the random variables can be transformed to the uncorrelated normal form by an eigenvalue problem as shown below.

5. COMPUTATIONAL ASPECTS

5.1. Random Variable Transformation

The mean and covariance can be obtained from the equations in Section 4. However, the number of derivatives to be evaluated is proportional to q(q+1)/2, where q is the number of random variables. To reduce computations, an eigenvalue orthogonalization procedure, which is similar to the modal analysis in structural dynamics, can be employed. The full covariance matrix $\mathrm{Cov}(b_i, b_j)$ is transformed to a diagonal variance matrix $\mathrm{Var}(c_i, c_j)$ such that

$$\mathrm{Var}(c_i, c_j) = 0 \qquad \text{for } i \neq j \tag{5-1}$$

and

$$\mathrm{Var}(c_i, c_j) = \mathrm{Var}(c_i) \qquad \text{for } i = j \tag{5-2}$$

Therefore, the number of evaluations is proportional to q. The above is achieved through the eigenproblem:

$$\Omega \Psi = \Psi \Lambda \tag{5-3}$$

where the Ω and Λ matrices denote Cov(b_i , b_j) and Var (c_i , c_j), respectively; Ψ is a constant q × q fundamental matrix with the following properties:

$$\Psi \Psi^T = \Psi^T \Psi = I \tag{5-4}$$

$$\Lambda = \Psi^T \Omega \Psi \tag{5-5}$$

and

$$\mathbf{b} = \Psi \mathbf{c} \qquad \text{or} \qquad \mathbf{c} = \Psi^T \mathbf{b} \tag{5-6}$$

I is the q × q identity matrix and **c** is the transformed q × 1 vector of random variables. Thus, the discretized random vector **b** is transformed to an uncorrelated random vector **c** with the variance of **c** as the eigenvalues of Ω in Eq. (5-3).

With Eqs. (5-5) and (5-6), the mixed derivatives appearing in Section 5 reduce to second derivatives and Var (b_i , b_j) reduces to Var (c_i). Thus, the mean of any function S[**b**(**x**), **x**] at any point x_k and the coveriance of the function between any two points x_k and x_m can be written as

$$E[S_k] = \bar{S}_k + \frac{1}{2} \sum_{i=1}^{q} \frac{\partial^2 \bar{S}_k}{\partial c_i^2} \mathrm{Var}(c_i) \tag{5-7}$$

and

$$\mathrm{Cov}[S_k , S_m] = \sum_{i\,j=1}^{q} \left(\frac{\partial \bar{S}_k}{\partial c_i} \right) \left(\frac{\partial \bar{S}_m}{\partial c_i} \right) \mathrm{Var}(c_i) \tag{5-8}$$

respectively.

It is observed that for one-dimensional random fields, as the correlation length increases from zero to a large value, the number of *largest* eigenvalues n, n ≤ q necessary to evaluate the mean and covariance in Eqs. (5-7) and (5-8) to a specified accuracy, decreases from q to 1. When the correlation length is zero the random field is uncorrelated and all q eigenvalues are dominant. As the field is uncorrelated, all q random variables are necessary to represent the randomness of the field. As the correlation length increases the number of dominant eigenvalues decreases. Eventually, for a very large correlation length the random field is closely correlated and there is just one dominant eigenvalue. As the field is closely correlated, only one random variable, corresponding to the largest eigenvalue, is sufficient to represent the randomness of the field. This feature, when present, can easily be exploited to reduce the computations. The value of n can be chosen based on the distribution of the eigenvalues before solving the PFEM equations. The eigenvalues here can be interpreted as weighting factors for the corresponding mode shapes necessary to represent the covariance structure; a large eigenvalue means a dominant mode and vice versa. Results of the eigenvalue distribution and selection of n, for beam problem and a bar problem, are discussed in Liu et al. (1986a, 1987).

5.2. Adjoint Method in PFEM

Consider a typical function Π(**c**, **d**) involving the displacements **d** and the random variables

c. Chain differentiation yields

$$[\Pi]_{c_i} = \Pi_{c_i} + \Pi_{\mathbf{d}}^{T} \mathbf{d}_{c_i}^{'} \tag{5-9}$$

where the subscript denotes the derivative with respect to c_i, and

$$\Pi_{\mathbf{d}}^{T} = (\Pi_{d_1}, \Pi_{d_2}, ..., \Pi_{d_{NEQ}}) \tag{5-10}$$

Using the first-order equation of PFEM in the transformed space, i.e.,

$$\mathbf{K}\, \mathbf{d}_i^{'} = \mathbf{f}_i^{'} \tag{5-11}$$

Eq. (5-9) becomes

$$[\Pi]_{c_i} = \Pi_{c_i} + \Pi_{\mathbf{d}}^{T} \mathbf{K}^{-1} \mathbf{f}_{c_i}^{'} \tag{5-12}$$

Usually, in the direct method, the above equation is evaluatedfor each random variable c_i, involving 'n' solutions of the linear equation (5-12). In the adjoint method, λ is selected to satisfy

$$\mathbf{K}\, \lambda = \Pi_{\mathbf{d}} \tag{5-13}$$

Then, Eq. (5-12) can be rewritten as

$$[\Pi]_{c_i} = \Pi_{c_i} + \lambda^{T} \mathbf{f}_{c_i}^{'} \tag{5-14}$$

The adjoint problem, Eq. (5-13), is solved only once in this method. In the direct method, 'n' solutions of Eq. (5-11) are required. This is the advantage of the adjoint method over the direct method. Both methods require 'n' inner products with $\mathbf{f}_{c_i}^{'}$ in Eqs. (5-9) and (5-14), respectively. However, it has been shown that when the number of functions is more than the number of random variables, the computational advantage of the adjoint method is lost (Liu et al., 1988d). By solving 'q' adjoint problems, the second order sensitivites can also be evaluated. It should be noted that the adjoint method is applicable to nonlinear problems as well, as the first and second order equations are still linear.

5.3 Parallel Computing in PFEM

Recent advances in computing hardware and software, have made multiprocessing in general and parallel processing in particular a viable and attractive technology. Parallel processing provides an opportunity to improve computing efficiency by orders of magnitude. Probabilistic computational mechanics exhibits several inherent levels of both coarse-and finite-grained parallelism. It is imperative to develop the computational strategies and algorithms to maximize

parallel processing efficiency and minimize parallel overhead. The parallelism in both the probabilistic computations and the structural mechanics computations has been explored by Sues et. al (1991,1992a). The implementation of parallel processing to general probabilistic structural analysis problems has been studied by Sues et al. (1991, 1992a). The parallel computing for probabilistic fatigue analysis has been implemented by Sues et al. (1992b) on both shared and distributed memory machines.

The parallel implementation of PFEM can be easily achieved in the solution of the first-order equations (sensitivity analysis). As shown from Eqs. (3-3)-(3-9), only one effective stiffness matrix needs to be formulated. Once the zeroth-order solution is obtained, q equations (Eq. (3-4)) can be solved in parallel to determine the response derivatives. Multiple levels of parallelism can be achieved if the substructuring (Komzsik and Rose, 1991), domain decomposition (Chan, et al., 1989) and operator splitting (Sues and Chen, 1992c) are also employed in PFEM.

6. APPLICATION OF PFEM TO THE RELIABILITY ANALYSIS OF BRITTLE FRACTURE AND FATIGUE

6.1 Introduction

In the previous section, the probabilistic finite element method, which is based on the second-order perturbation, has been formulated to quantify the statistical moments of the response of a stochastic system. In this section, the PFEM coupled with the first-order reliability method is developed to determine the reliability of brittle fracture and fatigue crack growth. The constrained optimization problem is formulated to calculate the reliability index. A Lagrange multiplier technique along with gradient projection algorithms is used to solve the constrained optimization problem.

Fracture and fatigue have become important factors in the structural design and safety of aging structures. The failure of an aging structure is usually resulted from microdefects activation, propagation, and formation of major cracks. Due to the ramdomness in the configuration of microdefects and uncertainty in the failure mechanism, the probabilistic fracture mechanics (PFM), which combines the fracture mechanics with the stochastic methods, provides a useful tool to address problems with large uncertainty.

The reliability analysis of flawed structures will here be classified into two groups of problems:

1. brittle material problems, where the material contains flaws with the random location and orientation. The major question is the reliability of the structure in the presence of these flaws.

2. ductile material problems, where failure is expected to result from the growth of a critical flaw until it can lead to failure of the structure.

The first category of the problem has been addressed recently by Lua et al. (1992a, 1992b) in quantifying the inherent statistical distribution of the fracture toughness of a multi-phase brittle material. The second question is of particular relevance to the safety of aging structures and nondestructive evaluation techniques. Because the threshold of detection is substantially greater than flaws sizes which may lead to failure over the course of time, inspection cycles should be set so that the reliability of an aging structure remains acceptable in these circumstances. Although a deterministic analysis can obtain an estimate of the fatigue life, the uncertainties in crack growth rates and the initial crack lengths detract from the usefulness of such solutions.

In this section, the application of the PFEM and the first-order reliability analysis for the brittle fracture and fatigue is presented. A brief review on the reliability methods is given first. The fusion of the PFEM and reliability analysis for probabilistic fracture and fatigue are then presented. Performance of the methodology developed is demonstrated on example problems.

6.2 Reliability Analysis

Reliability analysis is used to determine what is the likelihood that a structure subjected to uncertain loads, material properties and geometry, will satisfy a limit state criterion. Several text books and monographs on the methods and application of the reliability theory have been written, i.e. [Ditlevsen (1981), Ang and Tang (1984), Augusti et al. (1984), Madsen et al. (1986) and Melchers (1987)]. An overview of the first-order and seconder-order reliability methods (FORM/SORM), as well as various Monte Carlo simulation schemes has been given by Bjerager (1989). As the PFEM provides a powerful computational tool to determine first- and second-moment of random parameters, the second-moment reliability methods can be easily combined with the PFEM to obtain measures of the reliability of the structural systems.

Throughout this section the uncertainties-in load, material properties, component geometry and crack geometry- are represented by a q-dimensional vector of random variables denoted by $\mathbf{b} = [b_1, ..., b_q]^T$. A random variable reliability problem is described by a performance function, $g(\mathbf{b})$, which is a continuous measure of the ability of a system to perform as designed. Three states of a system, namely, the limit-state surface, the failure state, and the safe state, are defined by

$$g(\mathbf{b})=0 \qquad g(\mathbf{b})<0 \qquad \text{and} \qquad g(\mathbf{b})>0 \tag{6-1}$$

respectively. The probability of failure is given by

$$P_f = \int_{g(\mathbf{b})\le 0} f_{\mathbf{B}}(\mathbf{b})\, d\mathbf{b} \tag{6-2}$$

where $f_{\mathbf{B}}(\mathbf{b})$ is the multivariate density function of $\mathbf{b}$. Two difficulties are associated with Eq. (6-2). First, the domain of integration ($g(\mathbf{b}) \le 0$) is an implicit function of the random vector $\mathbf{b}$. Second, standard numerical integration of this multiple integral is prohibitively complicated as the number of random variables becomes large. Two approaches- MCS and failure surface approximation methods such as the first or second order reliability method (FORM or SORM)- have been employed extensively to calculate Eq. (6-2). In the first-order reliability method (FORM), the limit-state surface in the standard normal space is represented by the tangent hyperplane at the design point. In the second-order reliability method (SORM), the limit-state surface in the standard normal space is replaced by a quadratic surface, which is tangent at the design point. While MCS is completely general, it is very expensive and time-consuming for small probabilities of failure, which is the major concern in reliability engineering. FORM and SORM are more accurate and efficient for extreme probability of failure (e.g., 0.0001 or 0.9999 cumulative probability), however implementation can be more complex. In the present study, the FORM is applied to predict the reliability of a flawed component .

In order to make use of the properties of the standard normal space (rotationally symmetric and exponential decay), a transformation is introduced to map the original random variables $\mathbf{b}$ to a set of standard, uncorrelated normal variables $\mathbf{r}$. Eq. (6-2) in the $\mathbf{r}$-space becomes

$$P_f = \int_{\tilde{g}(r) \le 0} (2\pi)^{-q/2} \exp\left(-\frac{1}{2} \mathbf{r}^t \mathbf{r}\right) d\mathbf{r} \tag{6-3}$$

where $(\ )^t$ denotes the transpose of a vector or a matrix, and $\tilde{g}(\mathbf{r})$ (= $g(\mathbf{b}(\mathbf{r}))$) is the performance function in the transformed $\mathbf{r}$-space. FORM approximates the calculation in Eq.(6-3) as follows: first the point $\mathbf{r}^*$ on the limit-state surface ($\tilde{g}(\mathbf{r}) = 0$), which has the minimum distance to the origin, is found through an iterative algorithm, then the limit-state surface at the design point $\mathbf{r}^*$ is replaced with a tangent hyperplane given by

$$\tilde{g}(\mathbf{r}) \approx \frac{\partial \tilde{g}(\mathbf{r})}{\partial r_i} (r_i - r_i^*) \tag{6-4}$$

The resulting first order approximation to Eq. (6-3) is

$$P_{f1} \approx \int_{\frac{\partial \tilde{g}(\mathbf{r})}{\partial r_i} (r_i - r_i^*) \le 0} (2\pi)^{-q/2} \exp(-\frac{1}{2} \mathbf{r}^t \mathbf{r}) d\mathbf{r} = \Phi(-\beta) \tag{6-5}$$

where the reliability index β is defined by

$$\beta = \left(\mathbf{r}^{*t} \mathbf{r}^*\right)^{1/2} \tag{6-6}$$

and $\Phi(\ )$ is the standard normal cumulative probability. The step to determine the most probable point ($\mathbf{r}^*$)on the failure surface is the most critical in the reliability analysis. It generally requires to form an iteration and optimization scheme to calculate the gradients of the performance function.

In this paper, the reliability index β is determined by solving the following optimization problem in $\mathbf{r}$-space, i.e.,

$$\beta = \min (\mathbf{r}^T \mathbf{r})^{1/2}, \quad \text{subject to } g(\mathbf{r}) = 0 \tag{6-7}$$

The optimization can be solved using any general non-linear optimization algorithm such as HL-RF method (Hasofer and Lind, 1974; Hohenbichler and Rackwitz, 1981; Rackwitz and Fiessler, 1978), gradient projection method (Haug and Arora, 1979) and the modified HL-RF method (Der Kiureghian and Liu, 1988). A fast convergence rate is essential in selecting an iteration method.

The second order reliability method based on the second order Taylor expansion of the failure surface is given by Fiessler et al. (1979), Breitung (1984), Der Kiureghian et al. (1987), and Tvedt (1983).

6.3 Brittle Fracture Reliability Analysis

In order to model the singularity at the crack-tip, Bestfield et al (1990) used enriched element (Gifford and Hilton, 1978) . Other methods such as J-integral approach (Rice, 1968) and hybrid elements (Akin, 1976; Barsoum, 1976; Henshell and Shaw, 1975; Tong et al., 1973) can also be used. The enriched element approach has the advantage that mode I and II stress intensity factors, κ_I and κ_{II} are directly calculated along with the nodal displacement. This simplifies the development of the sensitivity equations which are needed in first-order reliability analysis.

The discretized global finite element equations are obtained by assembling the enriched elements that surround the crack-tip and the regular elements that model the remainder of the continuum. The global system of [neq + 2] equations (i.e., number of displacement equations plus mode I and II stress intensity factors) is

$$\mathbf{K(b)}\ \delta\mathbf{(b)}\ =\ \mathbf{f(b)} \tag{6-8}$$

where the generalized displacement, δ, and external force, **f**, vectors are

$$\delta\mathbf{(b)}\ =\ \begin{Bmatrix} \mathbf{d(b)} \\ \kappa\mathbf{(b)} \end{Bmatrix} \qquad \text{and} \qquad \mathbf{f(b)}\ =\ \begin{Bmatrix} \mathbf{h(b)} \\ \vartheta\mathbf{(b)} \end{Bmatrix} \tag{6-9}$$

respectively and the global stiffness matrix, $\mathbf{K(b)}$, is given by

$$\mathbf{K(b)}\ =\ \begin{bmatrix} \mathbf{R(b)} & \mathbf{C(b)} \\ \mathbf{C(b)}^{T} & \mathbf{E(b)} \end{bmatrix} \tag{6-10}$$

In Eqs. (6-8) through (6-10): **d** and **h** are the regular displacement and external force vectors, respectively; **R**, **E**, and **C** are the [neq × neq] regular stiffness matrix, the [2 × 2] stiffness matrix from the enriched terms, and the [neq × 2] coupled stiffness matrix from the regular and enriched terms, respectively. The other submatrices in Eq. (6-9) are

$$\kappa\mathbf{(b)}\ =\ \begin{Bmatrix} \kappa_{I}\mathbf{(b)} \\ \kappa_{II}\mathbf{(b)} \end{Bmatrix} \qquad \text{and} \qquad \vartheta\mathbf{(b)}\ =\ \begin{Bmatrix} f_{I}\mathbf{(b)} \\ f_{II}\mathbf{(b)} \end{Bmatrix} \tag{6-11}$$

where the two terms f_I and f_{II} are zero if the enriched element is not on a loaded boundary. Equations (6-8) through (6-11) are solved by condensing out the stress intensity factors (i.e., static condensation).

For mixed Mode I and Mode II fracture, several kinds of fracture criteria have been summarized by Wu and Li (1989). Among these criteria, the most widely used are: the maximum principal stress criterion proposed by Erdogan and Sih (1963) and the minimum strain energy density criterion, Sih (1974). In the case of mixed mode fatigue, the fatigue laws are generally based on an equivalent Mode I case to simulate actural mixed mode behavior. In order to be consistent with the mixed mode fatigue laws, the maximum principal stress criterion (Erdogan and Sih, 1963) is applied here to determine the equivalent Mode I stress intensity factor. Thus, the performance function for the mixed mode fracture can be expressed as

$$g\mathbf{(b)} = \kappa_c - \kappa_{eq} \tag{6-12}$$

Equation (6-12) implies that fracture occurs when the equivalent Mode I stress intensity factor, κ_{eq}, exceeds the critical value, κ_c. The direction of crack growth where the hoop stress becomes maximum is given by

$$Z(\kappa, \theta)\ =\ \Theta^{T}\ \kappa\ =\ 0 \tag{6-13}$$

where

$$\Theta = \begin{bmatrix} \sin\theta \\ 3\cos\theta - 1 \end{bmatrix} \tag{6-14}$$

In Eq.(6-14), θ is measured from the current crack line. The relation between the equivalent Mode I stress intensity factor (κ_{eq}) and stress intensity factor (κ_I, κ_{II}) is given by

$$\kappa_{eq} = \Phi^T \kappa \tag{6-15}$$

where

$$\Phi = \cos^2\left(\frac{\theta}{2}\right)\begin{bmatrix} \cos\frac{\theta}{2} \\ -3\sin\frac{\theta}{2} \end{bmatrix} \tag{6-16}$$

and θ is determined by Eq. (6-13). When only Mode I or Mode II fracture is present, Eq. (6-12) can be rewritten as

$$g(\mathbf{b}) = \kappa_c - \kappa_i, \qquad i = I, II \tag{6-17}$$

where κ_c is given by

$$\kappa_c = \kappa_{Ic} \quad \text{(for Mode I)} \quad \text{and} \quad \kappa_c = \frac{\sqrt{3}}{2}\kappa_{Ic} \quad \text{(for Mode II)} \tag{6-18}$$

In Eq. (6-18), κ_{Ic} stands for the fracture toughness. As indicated in Section (6.2), the determination of the reliability index for calculating the first-order probability of failure in the FORM is achieved by solving an optimization problem with one constraint (limit-state condition). In order to incorporate other constraints such as equation of equilibrium, crack direction law (in fatigue crack growth problem) in the formulation, the method of Lagrange multipliers can be applied. The statement of the optimization problem for brittle fracture is described in the following.

The nonlinear programming problem consists of determining the correlated random variables, $\mathbf{b} = [b_1, ..., b_q]^T$, and the generalized displacements, $\delta^T = [\mathbf{d}^T, \kappa^T]$, that minimize the distance from the origin to the limit-state surface in the independent standard normal space. The minimizer is termed as the reliability index β (Eq. (6-7)). The minimization is subject to the following equality constraint:

$$\mathbf{K}(\mathbf{b})\,\delta(\mathbf{b}) = \mathbf{f}(\mathbf{b}) \tag{6-19}$$

(i.e., equilibrium) and the following inequality constraint:

$$g(\mathbf{b}) \leq 0 \tag{6-20}$$

(i.e., the performance function being on the limit-state surface is a constraint in the optimization problem).

Equations (6-19), and (6-20) are converted to the Kuhn-Tucker problem (Arora 1989) by defining a Lagrange functional, L, of independent variables $\mathbf{b}$, δ, μ, λ, and α as follows

$$L(\mathbf{b}, \delta, \mu, \lambda, \alpha) = \mathbf{r}^T \mathbf{r} + \mu^T [\mathbf{f} - \mathbf{K}\,\delta] + \lambda\,[g + \alpha^2] \tag{6-21}$$

where μ is a Lagrange multiplier for equilibrium, $\lambda \geq 0$ is a Lagrange multiplier for the inequality constraint, and α is a slack variable that is introduced to ensure that $g \leq 0$. Depending on the sign of λ, the function to be minimized will increase or decrease with a change in g. In other words, if $\lambda \geq 0$, then $\mathbf{r}^T\mathbf{r}$ will decrease (i.e., minimize) while $g \leq 0$ (Converse 1970). The Kuhn-Tucker necessary conditions for the minimization of Eq. (6-21) are obtained by setting the derivatives of the Lagrange function with respect to the independent variables $\mathbf{b}$, δ, μ, λ, and α to zero, i.e.,

$$\frac{\partial L}{\partial \mathbf{b}} = \frac{\partial [\mathbf{r}^T \mathbf{r}]}{\partial \mathbf{b}} + \mu^T \left\{ \frac{\partial}{\partial \mathbf{b}} [\mathbf{f} - \mathbf{K}\,\delta] \right\} + \lambda \frac{\partial g}{\partial \mathbf{b}} = \mathbf{0} \tag{6-22}$$

$$\frac{\partial L}{\partial \delta} = -\mu^T \mathbf{K} + \lambda \frac{\partial g}{\partial \delta} = \mathbf{0} \tag{6-23}$$

$$\frac{\partial L}{\partial \mu} = \mathbf{f} - \mathbf{K}\,\delta = \mathbf{0} \tag{6-24}$$

$$\frac{\partial L}{\partial \lambda} = g + \alpha^2 \equiv 0 \tag{6-25}$$

$$\frac{\partial L}{\partial \alpha} = 2\,\lambda\,\alpha \equiv 0 \tag{6-26}$$

The optimization requires the solutions of Eqs. (6-22)-(6-26) for $\mathbf{b}$, δ, μ, $\lambda \geq 0$, and α. Equation (6-24) is simply equilibrium; and Eqs. (6-25) and (6-26) can be simplified to eliminate the slack variable, α, such that, $\lambda\, g = 0$ and $g \leq 0$ which ensures that $\lambda \geq 0$.

Since δ and $\mathbf{b}$ are independent variables in the Lagrange function (see Eq. (6-21)), the partial derivative of the second term with respect to $\mathbf{b}$ in Eq. (6-22) can be expressed as

$$\frac{\partial}{\partial \mathbf{b}} [\mathbf{f} - \mathbf{K}\delta] = \frac{\partial \mathbf{f}}{\partial \mathbf{b}} - \frac{\partial \mathbf{K}}{\partial \mathbf{b}}\delta \tag{6-27}$$

To simplify the right hand side of Eq. (6-27), the first-order probabilistic finite element equation (Eq. (3-4)) is employed for the present static problem, i.e.,

$$\mathbf{K} \frac{\partial \delta}{\partial \mathbf{b}} = \frac{\partial \mathbf{f}}{\partial \mathbf{b}} - \frac{\partial \mathbf{K}}{\partial \mathbf{b}}\delta \tag{6-28}$$

which yields

$$\frac{\partial}{\partial \mathbf{b}} [\mathbf{f} - \mathbf{K}\boldsymbol{\delta}] = \mathbf{K} \frac{\partial \boldsymbol{\delta}}{\partial \mathbf{b}} \tag{6-29}$$

when Eq. (6-28) is substituted into Eq. (6-27). Now multiplying each side of Eq. (6-29) by $\boldsymbol{\mu}^T$ and using Eq. (6-23) in the right hand side we obtain

$$\boldsymbol{\mu}^T \frac{\partial}{\partial \mathbf{b}} [\mathbf{f} - \mathbf{K}\boldsymbol{\delta}] = \lambda \frac{\partial g}{\partial \boldsymbol{\delta}} \frac{\partial \boldsymbol{\delta}}{\partial \mathbf{b}} \tag{6-30}$$

which can be expressed as

$$\boldsymbol{\mu}^T \frac{\partial}{\partial \mathbf{b}} [\mathbf{f} - \mathbf{K}\boldsymbol{\delta}] = \lambda \frac{\partial g}{\partial \boldsymbol{\kappa}} \frac{\partial \boldsymbol{\kappa}}{\partial \mathbf{b}} \tag{6-31}$$

since g is only a function of κ.

Substituting Eq. (6-31) into Eq. (6-22), the final optimization problem becomes

$$\mathbf{L}^{\beta} + \lambda \mathbf{L}^{g} = 0 \tag{6-32}$$

when $\lambda \geq 0$ where

$$\mathbf{L}^{g} = \frac{\partial g}{\partial \mathbf{b}} + \frac{\partial g}{\partial \kappa} \frac{\partial \kappa}{\partial \mathbf{b}} \tag{6-33}$$

$$\mathbf{L}^{\beta} = \frac{\partial}{\partial \mathbf{b}} [\mathbf{r}^T \mathbf{r}] \tag{6-34}$$

In Eqs. (6-34), $\frac{\partial}{\partial \mathbf{b}} [\mathbf{r}^T \mathbf{r}]$ is computed either explicitly or by finite difference depending if the random variables are normal or non-normal. In order to perform the sensitivity analysis on the stress intensity factors, namely, $\frac{\partial \kappa}{\partial \mathbf{b}}$, the probabilistic finite element method described in Sec. 3 can be applied to accomplish this task. Since we are only interested in the sensitivity of the stress intensity factors, considerable computational effort can be saved by using the adjoint method as described in Section 5.2. The iteration algorithm for the brittle fracture reliability is given by Besterfield et al. (1990).

In order to demonstrate the applicability of this approach to the brittle fracture reliability analysis, a single edge-cracked beam subjected to a concentrated point load is considered (see Fig. 7-5). The problem constants are given in Table 7-1. Due to symmetry, ten regular 9-node elements and two enriched 9-node elements are depicted in the left half of the beam as shown in Fig. 7-5. The applied load is modeled with one random variable with a coefficient of variation of 0.1 and the crack length is also modeled with one random variable and the coefficient of variation of 0.1. The convergence criterion for the optimization is 0.001. The variance of the Mode I stress intensity factor with randomness in force, material, crack length and the combination is presented in Table 7-2 for the adjoint method. Also presented in Table 7-2 are the summaries of the numerical performance and results of the reliability analysis (e.g., starting point, number of

iterations, the failure point, reliability index, and probability of failure). As shown in Table 7-2, the random crack length has less effect on the probability of failure due to the smaller variance for random crack length.

6.4 Fatigue Crack Growth Reliability Analysis

Fatigue crack growth is sensitive to many parameters and these parameters can seldom be determined accurately. Uncertainties in the crack geometry, material properties, crack direction, crack length, component geometry, and load time history all play a role. Thus, the prediction of fatigue failure must be treated as a probabilistic problem.

The first order second moment reliability method (FORM) can be applied to this problem as before by solving a constrained optimization problem. Due to the combined effects of external loading, unsymmetrical component geometry and crack geometry, cracks rarely grow in a straight line. Thus, the mixed-mode fatigue crack growth law and crack direction law should be employed.

The most common law for fatigue crack growth is the Paris-Erdogan model (1963), which gives the fatigue life, T, by

$$T = \int_{a_1}^{a_f} \frac{da}{D\,(\Delta\kappa_{eq})^n} \qquad (6\text{-}35)$$

where a_1 and a_f are the initial and final crack lengths, respectively, da is the random crack path; D and n are primarily material parameters but can also depend on the loading and environmental effects; and $\Delta\kappa_{eq}(a)$ is the range of equivalent Mode I stress intensity factors, i.e.,

$$\Delta\kappa_{eq} = \kappa_{eq}^{max} - \kappa_{eq}^{min} \qquad (6\text{-}36)$$

where κ_{eq}^{min} and κ_{eq}^{max} are the minimum and maximum equivalent Mode I stress intensity factors, respectively, associated with the minimum and maximum cyclic applied stresses, respectively. If the minimum equivalent Mode I stress intensity factor is assumed to be zero, then

$$\Delta\kappa_{eq} = \kappa_{eq}^{max} \equiv \kappa_{eq} \qquad (6\text{-}37)$$

The direction of the crack can be considered to be a random function, which will depend on the material properties and the history of the loading and the crack path. At each step, the statistics of the crack-tip, as reflected in this random function, in conjunction with the previous length of the crack and its orientation, will be used to obtain the new configuration. Based on the maximum hoop stress criterion (Erdogan and Sih, 1963), the crack growth direction $Z(\kappa, \theta)$ given by Eq. (6-13) is also employed here. Unlike the case of brittle fracture discussed before, the performance function for fatigue crack growth is given by

$$g = T - T_s \qquad (6\text{-}38)$$

where T_s is the service life of the component. In other words, the component fails when the fatigue life is less than the desired service life. The performance function could also be expressed in terms of a critical crack length.

The calculation of the reliability index by the first-order probability theory is performed in the same way as before by solving a constrained optimization problem. Before stating the optimization problem for fatigue crack growth, the crack direction law (Eq. (6-13)) must be discretized into "npts" discretization points along the crack path. At each crack path discretization point, the crack direction is

$$Z_k = \Theta_k^T \kappa_k = 0 \qquad k = 1, \ldots, \text{npts} \tag{6-39}$$

where κ_k and Θ_k represent κ and Θ evaluated at $\xi = \xi_k$, k = 1, ..., npts. Thus, at each crack path discretization point, the new crack direction is recalculated and the crack is then allowed to grow to the next discretization point.

The calculation of the reliability index by the first-order probability theory is posed as a constrained optimization problem. Unlike the previous brittle fracture reliability problem, both equality and inequality constrains have to be satisfied at each crack path discretization point. Also, the crack direction law (Eq. (6-39)) has to be included in the Lagrange function. By defining a Lagrange function, L, of independent variables $\mathbf{b}, \mu_1, \ldots, \mu_{npts}, \delta_1, \ldots, \delta_{npts}, \varphi_1, \ldots, \varphi_{npts}, \theta_1, \ldots, \theta_{npts}, \lambda$, and α, we have

$$L(\mathbf{b}, \mu_i, \delta_i, \varphi_i, \theta_i, \lambda, \alpha)$$

$$= \mathbf{r}^T \mathbf{r} + \sum_{i=1}^{npts} \mu_i^T [\mathbf{f}_i - \mathbf{K}_i \delta_i] + \sum_{k=1}^{npts} \varphi_k Z_k + \lambda \left\{ T - T_s + \alpha^2 \right\} \tag{6-40}$$

where μ_i is a Lagrange multiplier for equilibrium, φ_k is a Lagrange multiplier for the crack direction law, α is a slack variable which is introduced to ensure that $g \le 0$ and $\lambda \ge 0$ is a Lagrange multiplier for the inequality constraint.

The necessary conditions of Eq. (6-40) (i.e., derivatives with respect to the independent variables) then lead to

$$\frac{\partial L}{\partial \mathbf{b}} = \frac{\partial}{\partial \mathbf{b}} [\mathbf{r}^T \mathbf{r}] + \sum_{i=1}^{npts} \mu_i^T \frac{\partial}{\partial \mathbf{b}} [\mathbf{f}_i - \mathbf{K}_i \delta_i] + \sum_{k=1}^{npts} \varphi_k (Z_k)_{,\mathbf{b}} + \lambda T_{,\mathbf{b}} = \mathbf{0} \tag{6-41}$$

$$\frac{\partial L}{\partial \mu_i} = \mathbf{f}_i - \mathbf{K}_i\,\delta_i = 0 \qquad i = 1, \ldots, \text{npts}, \qquad \text{no sum on i} \tag{6-42}$$

$$\frac{\partial L}{\partial \delta_i} = -\,\mu_i^T\,\mathbf{K}_i + \sum_{k=1}^{\text{npts}} \varphi_k\,(Z_k)_{,\delta_i} + \lambda\,T_{,\delta_i} = \mathbf{0}$$

$$i = 1, \ldots, \text{npts}, \qquad \text{no sum on i} \tag{6-43}$$

$$\frac{\partial L}{\partial \lambda} = T - T_s + \alpha^2 = 0 \tag{6-44}$$

$$\frac{\partial L}{\partial \alpha} = 2\lambda\,\alpha = 0 \tag{6-45}$$

$$\frac{\partial L}{\partial \varphi_i} = Z_i = 0 \qquad i = 1, \ldots, \text{npts} \tag{6-46}$$

$$\frac{\partial L}{\partial \theta_i} = -\sum_{k=1}^{\text{npts}} \mu_k^T\,\frac{\partial \mathbf{K}_k}{\partial \theta_i}\,\delta_k + \sum_{k=1}^{\text{npts}} \varphi_k\,(Z_k)_{,\theta_i} + \lambda\,T_{,\theta_i} = 0$$

$$i = 1, \ldots, \text{npts} \tag{6-47}$$

where: $T_{,\mathbf{b}}$ in Eq. (6-41), $T_{,\delta_i}$ in Eq. (6-45), and $T_{,\theta_i}$ in Eq. (6-47) are the derivatives of the fatigue life T with respect to $\mathbf{b}$, δ_i, and θ_i, respectively, assuming $\mathbf{b}$, δ_i, and θ_i are independent variables; and $(Z_k)_{,\mathbf{b}}$ in Eq. (6-41), $(Z_k)_{,\delta_i}$ in Eq. (6-43), and $(Z_k)_{,\theta_i}$ in Eq. (6-47) are the derivatives of the crack direction law Z_k with respect to $\mathbf{b}$, δ_i, and θ_i, respectively, assuming $\mathbf{b}$, δ_i, and θ_i are independent variables. The optimization requires the solutions of Eqs. (6-41)-(6-47) for $\mathbf{b}$, $\mu_1, \ldots, \mu_{\text{npts}}$, $\delta_1, \ldots, \delta_{\text{npts}}$, α, $\lambda \geq 0$, $\varphi_1, \ldots, \varphi_{\text{npts}}$ and $\theta_1, \ldots, \theta_{\text{npts}}$. Equation (6-42) is simply equilibrium at each discretization point; Eq. (6-46) is the crack direction law at each discretization point; and Eqs. (6-44) and (6-45) can be simplified to eliminate the slack variable, α, such that $\lambda\,g = 0$ and $g \leq 0$, which ensures that $\lambda \geq 0$.

Since δ_i and $\mathbf{b}$ are independent variables in the Lagrange function [see Eq. (6-40)], the partial derivative of equilibrium with respect to the correlated random variables in Eq. (6-41) can be expressed as

$$\frac{\partial}{\partial \mathbf{b}}\,[\mathbf{f}_i - \mathbf{K}_i\,\delta_i] = \frac{\partial \mathbf{f}_i}{\partial \mathbf{b}} - \frac{\partial \mathbf{K}_i}{\partial \mathbf{b}}\,\delta_i \qquad \text{no sum on i}, \quad i = 1, \ldots, \text{npts} \tag{6-48}$$

To obtain an expression for the right hand side of Eq. (6-48), the first-order probabilistic finite

element equation (see Section 3) is employed, i.e.,

$$\mathbf{K}_i \frac{\partial \delta_i}{\partial \mathbf{b}} = \frac{\partial \mathbf{f}_i}{\partial \mathbf{b}} - \frac{\partial \mathbf{K}_i}{\partial \mathbf{b}} \delta_i \qquad \text{no sum on i,} \quad i = 1, \ldots, \text{npts} \tag{6-49}$$

which yields

$$\frac{\partial}{\partial \mathbf{b}} [\mathbf{f}_i - \mathbf{K}_i \delta_i] = \mathbf{K}_i \frac{\partial \delta_i}{\partial \mathbf{b}} \qquad \text{no sum on i,} \quad i = 1, \ldots, \text{npts} \tag{6-50}$$

when substituted into Eq. (6-48). Since $\delta_1, \ldots, \delta_{npts}$, and, $\theta_1, \ldots, \theta_{npts}$ are independent variables in the Lagrange function, Eqs. (6-43) and (6-47) simplify to:

$$- \mu_i^T \mathbf{K}_i + \varphi_i (Z_i)_{,\delta_i} + \lambda T_{,\delta_i} = 0 \qquad \text{no sum on i,} \quad i = 1, \ldots, \text{npts} \tag{6-51}$$

and

$$- \mu_i^T \frac{\partial \mathbf{K}_i}{\partial \theta_i} \delta_i + \varphi_i (Z_i)_{,\theta_i} + \lambda T_{,\theta_i} = 0 \qquad \text{no sum on i,} \quad i = 1, \ldots, \text{npts} \tag{6-52}$$

respectively. Multiplying each side of Eq. (6-50) by μ_i^T and substituting in Eqs. (6-51)-(6-52) yields

$$\mu_i^T \frac{\partial}{\partial \mathbf{b}} [\mathbf{f}_i - \mathbf{K}_i \delta_i] = \lambda \left\{ \frac{T_{,\delta_i} \mathbf{K}_i^{-1} \frac{\partial \mathbf{K}_i}{\partial \theta_i} \delta_i - T_{,\theta_i}}{(Z_i)_{,\theta_i} - (Z_i)_{,\delta_i} \mathbf{K}_i^{-1} \frac{\partial \mathbf{K}_i}{\partial \theta_i} \delta_i} (Z_i)_{,\delta_i} + T_{,\delta_i} \right\} \frac{\partial \delta_i}{\partial \mathbf{b}}$$

$$\text{no sum on i,} \quad i = 1, \ldots, \text{npts} \tag{6-53}$$

which can be expressed as

$$\mu_i^T \frac{\partial}{\partial \mathbf{b}} [\mathbf{f}_i - \mathbf{K}_i \delta_i] = \lambda \left\{ \frac{T_{,\delta_i} \mathbf{K}_i^{-1} \frac{\partial \mathbf{K}_i}{\partial \theta_i} \delta_i - T_{,\theta_i}}{(Z_i)_{,\theta_i} - (Z_i)_{,\delta_i} \mathbf{K}_i^{-1} \frac{\partial \mathbf{K}_i}{\partial \theta_i} \delta_i} (Z_i)_{,\kappa_i} + T_{,\kappa_i} \right\} \frac{\partial \kappa_i}{\partial \mathbf{b}}$$

$$\text{no sum on i,} \quad i = 1, \ldots, \text{npts} \tag{6-54}$$

since T and Z_i are only functions of κ_i, i = 1, ..., npts. After substituting Eqs. (6-52) and (6-54) into Eq. (6-41), the final form of the optimization for reliability for fatigue crack growth is given by

$$\mathbf{L}^{\beta} + \lambda\, \mathbf{L}^{g} = 0 \tag{6-55}$$

where

$$\mathbf{L}^{\beta} = \frac{\partial}{\partial \mathbf{b}} [\mathbf{r}^T \mathbf{r}] \tag{6-56}$$

$$\mathbf{L}^{g} = \sum_{i=1}^{npts} \left\{ \frac{T,_{\delta_i} \mathbf{K}_i^{-1} \dfrac{\partial \mathbf{K}_i}{\partial \theta_i} \delta_i - T,_{\theta_i}}{(Z_i),_{\theta_i} - (Z_i),_{\delta_i} \mathbf{K}_i^{-1} \dfrac{\partial \mathbf{K}_i}{\partial \theta_i} \delta_i} (Z_i),_{\kappa_i} + T,_{\kappa_i} \right\} \frac{\partial \kappa_i}{\partial \mathbf{b}}$$

$$+ \sum_{i=1}^{npts} \left\{ \frac{T,_{\delta_i} \mathbf{K}_i^{-1} \dfrac{\partial \mathbf{K}_i}{\partial \theta_i} \delta_i - T,_{\theta_i}}{(Z_i),_{\theta_i} - (Z_i),_{\delta_i} \mathbf{K}_i^{-1} \dfrac{\partial \mathbf{K}_i}{\partial \theta_i} \delta_i} (Z_i),_{\mathbf{b}} \right\} + T,_{\mathbf{b}} \tag{6-57}$$

In Eq. (6-57): $T,_{\mathbf{b}}$, $T,_{\kappa_i}$, $T,_{\theta_i}$, $T,_{\delta_i}$, $(Z_i),_{\mathbf{b}}$, $(Z_i),_{\kappa_i}$, $(Z_k),_{\theta_i}$, and $(Z_i),_{\delta_i}$ are determined explicitly in Reference (Besterfield et al., 1991). The sensitivity of the stress intensity factors, namely $\frac{\partial \kappa_i}{\partial \mathbf{b}}$, is also computed by the PFEM.

In order to demonstrate the performance of the method for reliability analysis against failure due to fatigue crack growth, a classical Mode I fatigue problem is presented. Figure 7-6 shows a finite rectangular plate with a single edge crack of length *a* subjected to a distributed load. The problem constants and second-moment statistics are given in Table 7-3. Due to symmetry, two enriched 9-node elements and twenty-three regular 9-node elements are depicted on the upper half of the plate. The reliability index is plotted versus the service life under the various types of uncertainties for the reference solution[13] and the solution obtained by PFEM in Figs. 7-7a and 7-7b, respectively. The same trends as the reference solution with the slight difference in the value of the reliability index can be observed through comparison of Fig. 7-7a with Fig.7-7b. This difference is due to the small numerical error in calculating the stress intensity factor by finite element methods. As shown in Fig.7-7a, for a service life of 4×10^6 cycles, the reliability index is less for uncertainty in the initial crack length (100 % coefficient of variation) and stress (25 % coefficient of variation) than for randomness in the final crack length (10 % coefficient of variation), fatigue parameter D (30 % coefficient of variation), and fatigue parameter n (2.5 % variation). When all five of the parameters are treated as random, the combined effect is much

greater than any one individual effect, as expected.

7. SBEM FOR THE CURVILINEAR FATIGUE CRACK GROWTH RELIABILITY ANALYSIS

7.1 Introduction

The development of probabilistic finite element method (PFEM) and its applications to linear, nonlinear structural mechanics problems and fracture mechanics problems have been discussed in the previous sections. In this section, we present a novel computational tool, called Stochastic Boundary Element Method (SBEM), for the reliability analysis of a curvilinear fatigue crack growth.

The SBIM based on the perturbation techniques has been developed by Ettouney et al. (1989) and Dasgupta (1992) for quantifying the statistic moments of tractions and displacements of a stochastic system. A general methodology, which combines the first order reliability method (FORM) with the mixed boundary integral equation method (Lua et al. , 1992c), has been formulated most recently by the authors (Lua et al., 1992d). The preformance and efficiency of the developed SBEM have been demonstrated by the problem of probabilistic fatigue crack growth.

The state-of-the-art of boundary element methods along with various of codes are given in the Boundary Element Reference Book (Mackerle and Brebbia, 1988). Due to its modelling efficiency and solution accuracy, BEMs have been used extensively in the field of computational fracture mechanics (Aliabadi and Rooke, 1991; Cruse, 1988). The application of the BEM to a curvilinear fatigue crack growth is presented in this section.

The curvilinear fatigue crack path is mainly attributed to the inherent inhomogeneity of the advance materials such as ceramics, composites or polycrystalline alloys. The existence of a micro-defect such as a void, a rigid inclusion or a transformation inclusion perturbs the stress field at a growing crack tip, resulting in a curvilinear crack path. In order to model the singularity at a moving crack tip, an automatic remeshing in conjunction with the quarter-point singular element (Barsoum, 1976; Henshall and Shaw, 1975) has been developed by Saouma (1984) to study the fatigue life of attachment lugs. A remeshing scheme based on the Arbitrary Lagrangian Eulerian (ALE) together with enriched finite elements has been developed by Besterfield (1991) in the reliability analysis of a fatigue crack growth. For problems of multiple fatigue cracks in which elastic interactions of a fatigue crack with micro-defects are treated, the remeshing scheme will be prohibitively complicated. The formulation based on the Boundary Integral Equations (BIEs) has several advantages in terms of solution accuracy and modeling efficiency.

Due to the degeneration of the usual displacement BIE for coplanar crack surfaces, the traction BIE has to be employed on the crack surface. The traction BIE alone is insufficient to solve the problem due to the coupling and interaction of the boundary of the component with the growing crack. Thus, the displacement BIEs have also to be applied. This set of mixed BIEs provide a unique solution for the boundary value problem. The application of the mixed BIEs to the elastic interactions of a fatigue crack and a micro-defect can be found in the Reference (Lua et al., 1992c).

By adding a few elements to permit crack extension along the crack growth direction, remeshing can almost be avoided. Similar to the approach used in enriched finite elements (Gifford and Hilton, 1987), a special interpolation function which incorporates the stress intensity factors is employed to model the near tip Crack Opening Displacements (CODs). The mixed BIEs are presented in Sec.7.2 for a multi-connected region with a fatigue crack. An enriched element which incorporates the mixed mode stress intensity factors is applied to characterize the singularity at a moving crack tip. The response gradient, which is key in FORM, is determined in Sec. 7.3 by direct differentiation. Due to the presence of three random processes in the expression of the response gradient, namely the mode I and mode II stress intensity factors and the crack direction

angle, the first order response-surface model is employed to determine the response sensitivity of these random processes. An iteration scheme based on the HL-RF method (Rackwitz and Fiessler, 1978) is employed to find the most probable failure point (or design point). Due to the high accuracy of the response gradient calculation based on the direct differentiation, fast convergence is obtained in the numerical iteration. The accuracy and efficiency of the present approach are demonstrated in Sec. 7.4 through a fatigue crack growth problem with randomness in the crack geometry, defect geometry, fatigue parameters and external loads.

7.2 Mixed BIEs for a Multi-Connected Region

Figure 7-8 shows a finite linear elastic body bounded by outer boundary Γ_o and inner boundaries Γ_i (i = 1, 2, ..., M), containing a finite crack under remote loading $\mathbf{t}^*$. A local Cartesian coordinate system (x',y') with origin at the center of the crack is employed with the y'-axis normal to the crack surface Γ_c. On the displacement boundary Γ_u, the displacement components u_i^* are prescribed; and on the remaining outer boundary Γ_t, the traction components t_i^* are given. The boundary conditions on the inner boundary $\Gamma_I \equiv \sum_{i=1}^{M} \Gamma_i$ can be specified based on the characteristics of a micro-defect (Lua et al., 1992c).

The usual displacement BIEs (see e.g. Telles, 1983) can be successfully applied on both inner boundary Γ_I and outer boundary Γ_o. The resulting BIEs on $\Gamma_I \cup \Gamma_o$ are

$$c_{ij}\, u_j(\zeta) = \int_{\Gamma_I+\Gamma_o} u^*_{ik}(\zeta;\mathbf{x})\, t_k(\mathbf{x})\, d\Gamma(\mathbf{x}) - \fint_{\Gamma_I+\Gamma_o} t^*_{ik}(\zeta;\mathbf{x})\, u_k(\mathbf{x})\, d\Gamma(\mathbf{x}) - T_{in} \int_{\Gamma_c} t'^*_{nk}(\zeta';\mathbf{x}')\, \Delta u'_k(\mathbf{x}')\, d\Gamma(\mathbf{x}')$$

$$\text{for } \zeta \in \Gamma_I \cup \Gamma_o \qquad (7\text{–}1)$$

where the symbol $\fint$ stands for the principal value of the integral in Cauchy's sense, and all the quantities with the prime ($'$) are defined in the local coordinate system; $t_k(\mathbf{x})$ and $u_k(\mathbf{x})$ are the components of traction and displacement, respectively, in the global coordinate system. $u^*_{ik}(\zeta;\mathbf{x})$ and $t^*_{ik}(\zeta;\mathbf{x})$ represent the displacement and traction, respectively, in the k-th direction at the field point $\mathbf{x}$ corresponding to a unit point force applied at the source point ζ in the i-th direction. Explicit expressions for these free space Green's functions are given in Telles (1983). The transformation from global to local coordinate system is given by the following transformation matrix $\mathbf{T}$ (or T_{in}):

$$\mathbf{T} = \begin{bmatrix} \cos\theta_0 & -\sin\theta_0 \\ \sin\theta_0 & \cos\theta_0 \end{bmatrix} \qquad (7\text{-}2)$$

The coefficient matrix c_{ij} depends on the smoothness of the boundary; $c_{ij} = \frac{1}{2}\delta_{ij}$ (for smooth boundary). The quantity $\Delta u'_m(\mathbf{x}')$ designates the COD on the crack surface Γ_c in the local coordinate system defined by

$$\Delta u'_m(x') = u^+_m(x') - u^-_m(x') \tag{7-3}$$

where $u^+_m(x')$ and $u^-_m(x')$ are the components of the displacement on the upper and lower crack surface, respectively. The coupling term representing the effect of CODs, which differs from the usual displacement BIEs, is the 3rd term in Eq. (7-1).

The displacement BIE (7-1) alone is insufficient to solve for all the unknowns, namely, the unknown displacement and traction on $\Gamma_I \cup \Gamma_o$ and CODs on Γ_c. Due to the degeneration of the displacement BIEs for coplanar crack surfaces, the higher order BIEs based on the traction boundary data on Γ_c is employed. Using the prescribed traction boundary condition on Γ_c, the resulting traction BIEs become

$$\bar{t}_i(\zeta) = n_j \{ \int_{\Gamma_I+\Gamma_o} u^*_{ijk}(\zeta;x)\, t_k(x)\, d\Gamma(x) - \int_{\Gamma_I+\Gamma_o} \psi^*_{ijk}(\zeta;x)\, u_k(x)\, d\Gamma(x) -$$
$$- T_{in}\, T_{js} \oint_{\Gamma_c} \psi'^*_{nk}(\zeta';x')\, \Delta u'_k(x')\, d\Gamma(x')\} \quad \text{for } \zeta \in \Gamma_c^+ \tag{7-4}$$

where the symbol ($\oint$) stands for the finite-part of a divergent integral, $\bar{t}_i$ are the prescribed traction components on the upper crack surface Γ_c^+, and $n_j=(\sin\theta_0, -\cos\theta_0)$ are the components of the normal vector to Γ_c^+ in the global coordinate system. The free space Green's function $u^*_{ijk}(\zeta;x)$ and $\psi^*_{ijk}(\zeta;x)$ are given by Lua et al (1992c).

In order to characterize the crack tip singularity, an enriched element which incorporates the stress intensity factors (SIFs) is used at the crack tip:

$$\Delta u'_1(s) = \frac{2(1-\nu)}{\mu}\frac{K_{II}}{\sqrt{\pi a}}\sqrt{2as-s^2}\ , \quad \Delta u'_2(s) = \frac{2(1-\nu)}{\mu}\frac{K_I}{\sqrt{\pi a}}\sqrt{2as-s^2} \tag{7-5}$$

where s is the distance behind the crack tip, a is the semi-crack-length, and K_I and K_{II} are mode I and mode II SIFs. In the numerical implementation of the mixed BIEs (Eqs. (7-1) and (7-4)), all the boundaries, namely Γ_I, Γ_o and Γ_c have to be discretized first. By dividing the boundary $\Gamma_I + \Gamma_o$ and the crack surface Γ_c into NE and NC elements, respectively, the discretized version of the mixed BIEs can be expressed as

$$c_{ij}\, u_j(\zeta) = \sum_{m=1}^{NE} \left[G^m_{ik}(\zeta;x_m)\, t^m_k - H^m_{ik}(\zeta;x_m)\, u^m_k\right] - \sum_{m=1}^{NC} Q^m_{ik}(\zeta';x'_m)\, \Delta u'^m_k$$
$$\text{for } \zeta = x_1, x_2, \ldots, x_{NE} \tag{7-6}$$

$$\bar{t}_i(\zeta) = n_j(\zeta) \left\{ \sum_{m=1}^{NE} \left[D^m_{ijk}(\zeta;x_m)\, t^m_k - S^m_{ijk}(\zeta;x_m)\, u^m_k\right] - \sum_{m=1}^{NC} R^m_{ijk}(\zeta';x'_m)\, \Delta u'^m_k \right\}$$
$$\text{for } \zeta = x_1, x_2, \ldots, x_{NC} \tag{7-7}$$

where the coefficient matrices G^m_{ik} , H^m_{ik} , Q^m_{ik} , D^m_{ijk} , S^m_{ijk} , and R^*_{ijk} are given by Lua et al (1992c).

7.3 FORM for the Curvilinear Fatigue Crack Growth

As described in Sec. 6.2, for the general correlated and non-normal random variables **b**, three steps are required in the first-order reliability analysis (FORM). They are: 1) transformation of **b** into the uncorrelated standard normal vector **r** by Rosenblatt transformation (Rosenblatt, 1952), 2) approximation of the failure surface in the **r**-space by a flat hyperplane at the most likely failure point (design point), 3) determination of the reliability index **b** by computing of the minimum distance from the origin to the limit state surface. As discussed in Sections 6.3-6.4, the design point has to be determined by an iterative optimization algorithm, which involves repeated computation of the limit state function (Eq. (6-1)) and its gradient. In order to ensure rapid convergence, an accurate determination of the response gradient is required.

Unlike the previous sections (6.3 and 6.4), where the response gradients or sensitivities have been determined by PFEM, the response gradients are calculated using SBEM. The direct differentiation coupled with the response-surface method is employed to perform the sensitivity analysis.

Assuming that the crack geometry $(a_i , a_f , x_0 , y_0 , \theta_0)$, fatigue parameters (D, n), external load (τ), and defect geometry (x_c , y_c , r_c , p_i) (see Fig.8) are modeled by a q-dimensional random vector **b**, the performance function for a fatigue problem is given by Eq. (6-38). Since the service life T_S is a deterministic variable, the gradient of the limit state function is given by the response sensitivity, i.e.,

$$\frac{\partial g}{\partial \mathbf{b}} = \frac{\partial}{\partial \mathbf{b}} T(\mathbf{b}, \kappa_{eq}(\mathbf{b})) \tag{7-8}$$

where T is given by Eq. (6-35). In order to facilitate the response gradient calculation, the line mapping is applied to map a curvilinear crack path to a local coordinate system, ξ ($\xi \in [-1, +1]$). The mapping function is defined by

$$a = \frac{1}{2}\left[(a_f - a_i)\,\xi + (a_f + a_i)\right] \tag{7-9}$$

Assuming that the crack geometry $(a_i , a_f , x_0 , y_0 , \theta_0)$, fatigue parameters (D, n), external load (τ), and defect geometry (x_c , y_c , r_c , p_i) (see Fig.8) are modeled by a q-dimensional random vector **b** (or **r** in the transformed space), and using Eqs. (6-37) and (7-9), Eq. (6-35) can be rewritten as

$$T(\mathbf{b}, \kappa_{eq}(\mathbf{b})) = \int_{-1}^{+1} f(\mathbf{b}, \kappa_{eq}(\mathbf{b}, \xi))\, d\xi \tag{7-10}$$

where the function f in Eq. (7-10) is given by

$$f(\mathbf{b}, \kappa_{eq}(\mathbf{b}, \xi)) = \frac{J(\mathbf{b})}{D\left[\kappa_{eq}(\mathbf{b}, \xi)\right]^n} \tag{7-11}$$

The Jacobian J in Eq. (7-11) is defined by

$$J(\mathbf{b}) = \frac{1}{2}(a_f - a_i) \tag{7-12}$$

Note that the function $\kappa_{eq}(\mathbf{b}, \xi)$ can be described only in an algorithmic form through the mixed BIEM (Eqs. (7-1) and (7-4)). This is the place where the mixed BIEM interfaces with the FORM to form the stochastic BIEM. Using Eqs. (7-10), (7-11) and (6-15), the total derivative of the response $(\frac{\partial T}{\partial \mathbf{b}})$ is given by

$$\frac{\partial T}{\partial \mathbf{b}} = \int_{-1}^{+1} \left[f_{,\mathbf{b}} + f_{,\kappa_{eq}} \left(\kappa_{eq,\kappa_I} \frac{\partial \kappa_I(\mathbf{b}, \xi)}{\partial \mathbf{b}} + \kappa_{eq,\kappa_{II}} \frac{\partial \kappa_{II}(\mathbf{b}, \xi)}{\partial \mathbf{b}} + \kappa_{eq,\theta} \frac{\partial \theta(\mathbf{b}, \xi)}{\partial \mathbf{b}} \right) \right] d\xi \tag{7-13}$$

where κ_{eq,κ_I}, $\kappa_{eq,\kappa_{II}}$ and $\kappa_{eq,\theta}$ are derived from Eq. (6-15) and given by

$$\kappa_{eq,\kappa_I} = \cos^3 \frac{\theta}{2} \tag{7-14}$$

$$\kappa_{eq,\kappa_{II}} = -3 \cos^2 \frac{\theta}{2} \sin \frac{\theta}{2} \tag{7-15}$$

$$\kappa_{eq,\theta} = \frac{3}{2} \cos\frac{\theta}{2} \left[-\cos\frac{\theta}{2} \sin\frac{\theta}{2} \kappa_I + \left(2 \sin^2 \frac{\theta}{2} - \cos^2 \frac{\theta}{2} \right) \kappa_{II} \right] \tag{7-16}$$

Both $f_{,\mathbf{b}}$ and $f_{,\kappa_{eq}}$ in Eq. (7-13) can be determined explicitly from Eq. (7-11). The results are

$$f_{,\mathbf{b}} = \frac{1}{D (\kappa_{eq})^n} \frac{\partial J}{\partial \mathbf{b}} - \frac{J}{D^2 (\kappa_{eq})^n} \frac{\partial D}{\partial \mathbf{b}} - \frac{J \ln(\kappa_{eq})}{D (\kappa_{eq})^n} \frac{\partial n}{\partial \mathbf{b}} \tag{7-17}$$

$$f_{,\kappa_{eq}} = - \frac{n J (\kappa_{eq})^{-(n+1)}}{D} \tag{7-18}$$

Due to both the complicated explicit expressions and implicit functions involved in Eq. (7-13), numerical integration is required to calculate the response sensitivity (Eq.(7-13)). By dividing the integration interval [-1, +1] into Npts-1 line elements, which correspond to Npts-1 crack growth steps, and applying the trapezoidal rule, Eq. (7-13) can be approximated by

$$\frac{\partial T}{\partial \mathbf{b}} \approx \sum_{n=1}^{Npts} \left[f_{,\mathbf{b}} + f_{,\kappa_{eq}} \left(\kappa_{eq,\kappa_I} \frac{\partial \kappa_I(\mathbf{b}, \xi)}{\partial \mathbf{b}} + \kappa_{eq,\kappa_{II}} \frac{\partial \kappa_{II}(\mathbf{b}, \xi)}{\partial \mathbf{b}} + \kappa_{eq,\theta} \frac{\partial \theta(\mathbf{b}, \xi)}{\partial \mathbf{b}} \right) \right]_{\xi_n} W_n \tag{7-19}$$

where $\xi_n = -1 + 2(n-1)/(Npts-1)$, and W_n are the integration weights given by

$$W_n = \frac{1}{Npts - 1} \text{ (for n=1 or n=Npts)} , \quad W_n = \frac{2}{Npts - 1} \text{ (otherwise)} \tag{7-20}$$

Since κ_I, κ_{II} and θ are implicit functions of both $\mathbf{b}$ and ξ in Eq. (7-19), the direct calculation of

these response sensitivities, namely, $\frac{\partial \kappa_I}{\partial \mathbf{b}}$, $\frac{\partial \kappa_{II}}{\partial \mathbf{b}}$ and $\frac{\partial \theta}{\partial \mathbf{b}}$ is not feasible in this case.

As shown in Eq. (7-19), the key step in the implementation of stochastic BIEM for a curvilinear fatigue crack growth reliability is to determine three response sensitivities ($\frac{\partial \kappa_I}{\partial \mathbf{b}}$, $\frac{\partial \kappa_{II}}{\partial \mathbf{b}}$ and $\frac{\partial \theta}{\partial \mathbf{b}}$) at each integration point ξ_n (n= 1, 2, ..., Npts). In addition to the implicit dependence of functions $\kappa_I(\mathbf{b}, \xi)$, $\kappa_{II}(\mathbf{b}, \xi)$ and $\theta(\mathbf{b}, \xi)$ on both **b** and ξ, these three functions represent three random processes due to the presence of the random vector **b**. Since $\kappa_I(\xi)$, $\kappa_{II}(\xi)$ and $\theta(\xi)$ at a given realization of **b** can be easily generated by using the mixed BIEM (see Sec. 7.2), the response-surface approach (Faravelli (1989, 1986)) is employed to determine the response sensitivity $\left(\frac{\partial \kappa_I}{\partial \mathbf{b}}, \frac{\partial \kappa_{II}}{\partial \mathbf{b}} \text{ and } \frac{\partial \theta}{\partial \mathbf{b}}\right)$ at each discretization point ξ_n (n =1, 2,..., Npts). The first order response model in **b** is employed in conjunction with factorial experiments with each factor at two levels (Myers, 1971). As $\kappa_I(\mathbf{b}, \xi)$, $\kappa_{II}(\mathbf{b}, \xi)$ and $\theta(\mathbf{b}, \xi)$ are independent of the fatigue parameters, D and n, the dimension of **b** in κ_I, κ_{II} and θ is q-2.

With the help of the deterministic solver based on the mixed BIEM, 2^{q-2} computer simulations are performed in accordance with predefined factorial simulations. By performing the least squares fitting process at each crack path discretization point ξ_n (n =1, 2, ..., Npts), the history of the response sensitivity of $\frac{\partial \kappa_I(\mathbf{b}, \xi)}{\partial \mathbf{b}}$ $\left(\frac{\partial \kappa_I(\mathbf{b}, \xi_n)}{\partial \mathbf{b}} \text{ and } \frac{\partial \theta(\mathbf{b}, \xi_n)}{\partial \mathbf{b}}\right)$ at the L-th iteration, $\mathbf{b}^L$ can be determined. Substituting the results $(\frac{\partial \kappa_I(\mathbf{b}, \xi_n)}{\partial \mathbf{b}}, \frac{\partial \kappa_{II}(\mathbf{b}, \xi_n)}{\partial \mathbf{b}} \text{ and } \frac{\partial \theta(\mathbf{b}, \xi_n)}{\partial \mathbf{b}}$; n = 1, 2, ..., Npts) into Eq. (7-19), the sensitivity of the fatigue life T with respect to the primary random vector **b** at $\mathbf{b}^L$ can be determined. For a given service life T_s, an iterative algorithm to obtain the location of the design point $\mathbf{b}^*$, the response sensitivity at the design point $\left[\frac{\partial T}{\partial \mathbf{b}}\right]_{\mathbf{b}^*}$ and the reliability index (or the probability of failure) can be found in the Reference (Lua et al., 1992d).

7.3 Numerical Results

In order to show the accuracy and efficiency of the stochastic BIEM in a curvilinear fatigue crack reliability setting, a single edge-cracked plate with a random transformation inclusion is considered (see Fig. 7-9). The plate geometry (W, L), initial crack location (x_0 , y_0), initial crack angle (θ_0), final crack size (a_f), and material constants (aluminum 7075-T651) are deterministic parameters given by

$$L = W = 2.0 \text{ in}, x_0 = -1.0 \text{ in}, y_0 = 0.0 \text{ in}, \theta_0 = 0.0 \tag{7-21}$$

$$a_f = 0.5 \text{ in}, \mu = 3.866 \times 10^6 \text{ psi}, \nu = 0.33 \tag{7-22}$$

where μ is the shear modulus and ν is the Poisson's ratio. The crack geometry (a_i), external load (τ), fatigue parameters (D, n), the defect geometry (x_c , y_c , r_c), and the internal pressure (p_i) resulting from the residual strain in the inclusion are assumed to be independent random variables with specified probability density functions.

The statistical parameters of random input variables (mean, standard deviation and coefficient of variance (COV)) along with corresponding distribution functions are listed in Table

1. As shown in Table 4, the initial crack size a_i has the largest dispersion (COV =60%). For the initial crack length a_i, a uniform distribution with a tail is employed here (see Fig. 7-10). The detection threshold, which is equal to 7.5×10^{-3} shown in Fig. 7-10, represents the lower limit of an inspection device to detect the presence of a small crack. Below the detection threshold the probability density is assumed uniform; above the threshold the probability density decays linearly to zero, representing false negatives of the inspection technique. For the purpose of verifying the accuracy of the stochastic BIEM, the Monte Carlo Simulation (MCS) for the sample size $N_s = 2000$ is used.

The Cumulative Distribution Function (CDF) of the fatigue life T obtained by the stochastic BIEM for values of service life T_s are presented in Fig. 7-11. The agreement of MCS and SBIEM results shown in Fig.7-11 demonstrates the accuracy and efficiency of the stochastic BIEM. As a rule of thumb (Bjerager, 1989), the sample size necessary for MCS to get a probability estimate with good confidence is around $100/p_f$. For small probabilities of failure $p_f (\approx 10^{-3} - 10^{-6})$, which are the major interest in reliability engineering, one needs $10^5 - 10^8$ Monte Carlo simulations to achieve good confidence. The number of iterations in the stochastic BIEM required to find the design point $\mathbf{b}^*$ is only of order 15 to 20 for $\beta \approx 3 - 5$ (or $p_f = 0.001 - 0.3 \times 10^{-6}$). Therefore the stochastic BIEM based on FORM has an overwhelming advantage over the MCS for small probabilities of failure in terms of solution accuracy and efficiency.

The reliability index (β) versus the service life (T_s) is shown in Fig. 7-12 along with the results of no micro-defect. As shown in Fig. 7-12, the presence of a random transformation inclusion has a detrimental effect on the fatigue life. The comparison of response sensitivities at Most-Probable-Points (MPPs or design points) versus the probability of failure for both cases is plotted in Fig. 7-13. As shown in Fig. 7-13, the presence of a random transformation inclusion changes the response sensitivity of a_i significantly. The comparison of the loci of the Most-Probable-Point (MPP) of crack geometry (a_i) is shown in Fig. 7-14. Due to the presence of the random transformation inclusion, the locus of MPP of a_i changes considerably as shown in Fig. 7-14. When the value of a_i increases, the probability of failure p_f becomes large (see Fig. 14). This is the main reason why the routine crack inspection is so important to avoid the large probability of failure.

8. Conclusions

The Probabilistic Finite Element Method (PFEM) is presented, which is based on the second-order perturbation. Due to the discrete nature of the finite element formulation, the random field has to be also discretized. Existing approaches for representation of random fields are outlined. To the efficient characterization of the random field, the transformation of the original random variables into a set of uncorrelated random variables is introduced through an eigenvalue orthogonalization procedure. Both single-field variational principle and three-field Hu-Washizu variational principle are employed to develop the PFEM for linear, and nonlinear problems, respectively. The computational aspects in the numerical implementation of the PFEM are also presented.

The accuracy and efficiency of PFEM in quantifying the statistic moments of a stochastic system are demonstrated through two examples: 1) a stochastic spring-mass system under sinusoidal excitation; 2) a cantilever beam subjected to large deflection. The results are in good agreement with Monte Carlo simulations (MCSs). The computational efficiency of PFEM far exceeds MCS. Since the PFEM developed essentially involve solution of a set of deterministic problem, it is easily integrable into any FEM based code.

The PFEM coupled with the first-order reliability method is alsopresented for the reliability analysis of both fracture and fatigue. The methodology consists of calculating the reliability index via an optimization procedure, which is used to calculate the probability of failure. The PFEM provides a powerful tool for the sensitivity analysis, which is required in an iterative optimization algorithm. Performance of the methodology presented is demonstrated on a single edge-cracked beam with a concentrated load and a classical mode I fatigue crack growth problem.

In addition to the PFEM, the stochastic boundary element method (SBEM), which combines the mixed boundary integral equation with the first-order reliability method, is also presented for the curvilinear fatigue crack reliability analysis. Due to the high degree of complexity and nonlinearity of the response, direct differentiation coupled with the response-surface method is employed to determine the response gradient. The reliability index and the corresponding probability of failure are calculated for a fatigue crack growth problem with randomness in the crack geometry, defect geometry, fatigue parameters and external loads. The response sensitivity of each primary random variable at the design point is also determined to show its role in the fatigue failure. The results show that the initial crack length is a critical design parameter. Since crack lengths below the threshold of an inspection limit are likely to exhibit a large amount of scatter, this makes it imperative that the life expectancy of a strycture be treated from a stochastic viewpoint.

Probabilistic analysis is becoming increasingly important for the safety and reliability of an aging structure and for tailoring new advanced materials. Due to the complexity in charactrizing material behavior, structural response, and failure mechanism, probabilistic mechanics problems are computationally intensive and strain the resources of currently available computers. Since many sources of parallelism are inherent in probabilistic mechanics problems, it is evident that the development of a parallel computing enviroment for probabilistic response analysis in the current trend in stochastic computational mechanics.

References

1) Akin, J.E.1976. The Generation of Elements with Singularities. Int. J. Numer. Methods Eng., **10**, pp. 1249-1259.

2) Aliabadi, M.H. and Rooke, D.P. 1991. Numerical Fracture Mechanics. Computational Mechanics Publishers, Southampton/Boston.

3) Ang, A.H.S. and Tang, W.H. 1984. Probability Concepts in Engineering Planning and Design: Volume II - Decision, Risk, and Reliability . John Wiley & Sons, New York.

4) Arora, J.S. 1989. Introduction to Optimal Design, McGraw-Hill, New York, pp. 122-136.

5) Augusti, G., Baratta, A. and Casciati, F.1984. Probabilistic Methods in Structural Engineering. Chapman and Hall, London.

6) Baecher, G. B. and Ingra, T.S. 1981. Stochastic FEM in settlement predictions. Journal of the Geotechnical Engineering Division, ASCE, 107 (GT4), pp. 449-63.

7) Barsoum, R.S. 1976. On the Use of Isoparametric Finite Elements in Linear Fracture Mechanics. Int. J. Numer. Methods Eng. . **10**, pp. 25-37.

8) Belytschko, T. et al. 1984. Hourglass Control in Linear and Nonlinear Problems. Comput. Methods Appl. Mech. Eng. **43**, pp. 251-276.

9) Belytschko, T. and Bachrach, W.E. 1986. Simple Quadrilateral with High-Course Mesh Accuracy. Comput. Methods Appl. Mech. Eng. **54**, pp.279-301.

10) Benaroya, H. and Rehak, M. 1988. Finite element methods in probabilistic structural analysis. Appl. Mech. Rev. **41** (5), 201-213.

11) Besterfield, G.H., Liu, W.K., Lawrence, M.A., and Belytschko, T.B. 1990. Brittle Fracture Reliability by Probabilistic Finite Elements. J. Eng. Mech. ASCE **116** pp. 642-659.

12) Besterfield, G.H., Liu, W.K., Lawrence, M. and Belytschko, T. 1991. Fatigue Crack Growth Reliability by Probabilistic Finite Elements. Comput. Methods Appl. Mech. Eng. **86**, pp. 297-320.

13) Bjerager, P. 1989. Probability Computation Methods in Structural and Mechanical Reliability. Computational Mechanics of Probabilistic and Reliability Analysis, Liu, W.K. and Belytschko, T. eds., Elme Press International, pp. 47-68.

14) Breitung, K. 1984. Asymptotic Approximation for Multinormal Integrals. J. Eng. Mech. ASCE, **110**, pp. 357-366.

15) Cambou, B. 1975. Application of first-order uncertainty analysis in the finite element method in linear elasticity. Proceedings of the 2nd International Conference on Application of Statistics and Probability in Soil and Structural Engineering, Aachen, West Germany, Deutsche Gesellschaft fur Grd-und Grundbau ev, Essen, FRC, pp. 67-87.

16) Chan, T.F., Glowinski, R., Periaux, J., Widlund, O. 1989. Domain decomposition methods for partial differential equations. SIAM, Philadelphia, PA.

17) Converse, A. O. 1970. Optimization Robert Krieger Publishing Co., New Yprk, pp 243-248.

18) Cruse, T. A., Wu, Y.-T., Dias, B., and Rajagopal, K. R. 1988a. Probabilistic structural analysis methods and applications. Comput. Struct. **30**, pp. 163-170 .

19) Cruse, T.A. 1988b. Boundary Element Analysis in Computational Fracture Mechanics. Kluwer Academic Publishers.

20) Dasgupta, G. 1992. Stochastic finite and boundary element simulations. Proceeding of the Sixth Specialty Conference, Denver, Colorado, July 8-10, pp. 120-123.

21) Der Kiureghian, A. 1985. Finite Element Methods in Structural Safety Studies. Proc ASCE Convention, Denver, May.

22) Der Kiureghian, A. and Ke, B.-J. 1985. Finite-element based reliability analysis of frame structures. Proceedings, Fourth International Conference on Structural Safety and Reliability, Kobe, Japan, I, pp. 395-404.

23) Der Kiureghian, A., Lin, H.- Z., and Hwang, S. J. 1987. Second-Order Reliability Approximations. J. Eng. Mech., ASCE, **113**, pp. 1208-1225.

24) Der Kiureghian, A. and Ke, B.-J. 1988a. The Stochastic Finite Element Method in Structural Reliability. Probabilistic Engineering Mechanics **3**, pp. 83-91.

25) Der Kiureghian, A. and Liu, P.-L. 1988b. Optimization Algorithms for Structural Reliability. Computational Probabilistic Mechanics ADM-93, ASME, pp. 185-196.

26) Ditlevsen, O. 1981. Uncertainty Modeling with Applications to Multidimensional Civil Engineering Systems, McGraw-Hill Inc., New York.

27) Erdogan, F. and Sih, G.H. 1963. On the Crack Extension in Plates under Plane Loading and Transverse Shear. J. Basic Eng., ASME, **85**, pp. 519-527.

28) Ettouney, M., Benaroya, H., and Wright, J. 1989. Probabilistic Boundary Element Methods. Computational Mechanics of Probabilistic and Reliability Analysis, Liu, W.K. and Belytschko, T. eds., Elme Press International, pp. 142-165.

29) Fiessler, B., Neumann, H.-J. and Rackwitz, R. 1979. Quadratic Limit States in Structural Reliability. J. Eng. Mech. ASCE, **105**, pp. 661-676.

30) Fraravelli, L. 1986. A response surface approach for reliability analysis. RILEM Symp on Stoch. Meth. in Mat. and Struct. Eng. .

31) Faravelli, L. 1989. Response surface approach for reliability analysis. J. Eng. Mech. ASME **115**, pp. 2763-2781.

32) Gifford, L.N. and Hilton, P.D. 1978. Stress Intensity Factors by Enriched Finite Elements. Engng Fracture Mechanics **10**, pp. 485-496.

33) Grigoriu, M. 1982. Methods for approximate reliability analysis. Structural Safety **1**, pp. 155-165.

34) Handa, K. and Andersson, K. 1981. Application of finite element methods in the statistical

analysis of structures. Proceedings of the 3rd International Conference on Structural Safety and Reliability, Elsevier, Amsterdam, pp. 409-417.

35) Hasofer, M. and Lind, N.C. 1974. Exact and Invariant Second-Moment Code Format. *J.* Eng. Mech. ASCE, **100**, pp.111-121.

36) Haug, E.J. and Arora, J.S. 1979. Applied Optimal Design: Mechanical and Structural Systems, 1st ed., John Wiley & Sons, New York, pp. 319-328.

37) Henshell, R.D. and Shaw, K.G. 1975. Crack Tip Elements Are Unnecessary. Int. J. Numer. Methods Eng. **9**, pp. 495-507.

38) Hisada, T. and Nakagiri, S. 1981. Stochastic finite element method developed for structural safety and reliability. Proceedings of the 3rd International Conference on Structural Safety and Reliability, Elsevier, Amsterdam, pp. 395-408.

39) Hisada, T. and Nakagiri, S. 1985. Role of the Stochastic Finite Element Method in Structural Safety and Reliability. Proceedings, 4th International Conference on Structural Safety and Reliability, Kobe, Japan, pp. 385-394.

40) Hohenbichler, A.M. and Rackwitz, R. 1981. Non-Normal Dependent Vectors in Structural Safety. J. Eng. Mech., ASCE, **107**, pp. 1227-1238.

41) Komzsik, L. and Rose, T. 1991. Substructuring in MSC/NASTRAN for large scale parallel applications Computer Systems in Engineering. **2** (2/3), pp. 167-173.

42) Lawrence, M.A. 1987. Basis Random Variables in Finite Element Analysis Int. J. Numer Method Eng. **24**, pp. 1849-1863.

43) Liu, P.-L. and Der Kiureghian, A. 1991. Finite element reliability of geometrically nonlinear uncertain structures. J. Eng. Mech. ASCE **117** (8), 1806-1825 .

44) Liu, W.K., Belytschko, T. and Mani, A. 1986a. Random Field Finite Elements. Int. J. Numer. Methods Eng. **23**, pp. 1831-1845.

45) Liu, W.K., Belytschko, T. and Mani, A. 1986b. Probabilistic Finite Elements for Nonlinear Structural Dynamics. Comput. Methods Appl. Mech. Eng **56**.

46) Liu, W.K., Belytschko, T. and Mani 1987. Applications of Probabilistic Finite Element Methods in Elastic/Plastic Dynamics. J. Eng. Ind. ASME, **109**, pp.2-8.

47) Liu, W.K., Besterfield, G.H. and Belytschko, T. 1988a. Variational Approach to Probabilistic finite Elements. J. Eng. Mech. ASCE, **114**, pp. 2115-2133.

48) Liu, W.K., Besterfield, G.H. and Belytschko, T. 1988b. Transient probabilistic systems. Compt. Methods Appl. Mech. Eng. **67**, pp. 27-54.

49) Liu, W.K., Belytechko, T. and Chen, J.S. 1988c. Nonlinear version of flexurally superconvergent element. Comput. Methods Appl. Mech. Eng. **71**, pp. 241-258.

50) Liu, W.K., mani, A. and Belytschko, T. 1988d. Finite element methods in probabilistic mechanics. Probabilistic Eng. Mech. **2** (4), pp. 201-213.

51) Liu, W.K. and T. Belytschko 1989. Computational Mechanics of Probabilistic and

Reliability Analysis Elme Press International.

52) Lua, Y.J, Liu, W.K. and Belytschko, T. 1992a. A Stochastic Damage Model for the Rupture Prediction of a Multi-Phase Solid: Part I: Parametric Studies. Int. J. Fracture Mech. **55**, pp. 321-340 .

53) Lua, Y.J, Liu, W.K. and Belytschko, T. 1992b. A Stochastic Damage Model for the Rupture Prediction of a Multi-Phase Solid: Part II: Statistical Approach. Int. J. Fracture Mech. **55**, pp. 341-361 .

54) Lua, Y. J. , Liu, W.K., and Belytschko, T. 1992c. Elastic interactions of a fatigue crack with a microdefect by the mixed boundary integral equation method. submitted to Int. J. Numer. Methods Eng.

55) Lua, Y.J., Liu, W. K., and Belytschko, T. 1992d. Curvilinear fatigue crack reliability analysis by stochastic boundary element method. submitted to Int. J. Numer. Methods Eng.

56) Ma, F. 1986. Approximate Analysis of a Class of Linear Stochastic Systems with Colored White Noise Parameters. Int. J. Eng. Sci. **24** (1), pp. 19-34.

57) Mackerle, J. and Brebbia, C.A. 1988. The Boundary Element Reference Book Computational Mechanics Publications, Southampton, Boston.

58) Madsen, H.O., Krenk, S. and Lind, N.C. 1986. Methods of Structural Safety, Prentice-Hall, Inc., Englewood Cliffs, N.J.

59) Melchers, R.E. 1987. Structural Reliability, Analysis and Predictions, Ellis Horwood Series in Civil Engineering, Halsted Press, England.

60) Myers, R.H. 1971. Response Surface Methodology. Allyn and Bacon Inc., Boston.

61) Noor, A. K. 1991. Bibligraphy of books and monographs on finite element technology. Appl Mech Rev **44** (6), pp. 307-317.

62) Paris, P.C. and Erdogan, F. 1963. A Critical Analysis of Crack Propagation Laws. J. Basic Eng. ASME, **85**, pp. 528-534.

63) Rackwitz, R. and Fiessler, B. 1978. Structural Reliability under Combined Load Sequences. Comput. Struct. **9**, pp. 489-494.

64) Rice, J.R. 1968. A Path Independent Integral and the Approximate Analysis of Strain Concentrations by Notches and Cracks. J. Appl. Mech. ASME, **35**, pp. 379-386.

65) Rosenblatt, M. 1952. Remarks on a multivariate transformation. Annals of Mathematical Statistics. **23**, pp. 470-472.

66) Saouma, V.E. 1984. An automated finite element procedure for fatigue crack propagation analysis. Engng Fracture Mech. **20**, pp. 321-333.

67) Shinozuka, M. 1987. Stochastic fields and their digital simulation. Stochastic Methods in structural Dynamics, Schuellernd, C.I. and Shinozuka, M. eds., Martinus Nijhoff Publishers, Boston, pp. 92-133.

68) Shinozuka, M. and Deodatis, G. 1988a. Response variability of stochastic finite element

systems. J. Engng. Mech., ASCE, **114** (3), pp. 499-519.

69) Shinozuka, M and Yamazaki, F. 1988b. Stochastic finite element analysis: an introduction. in Stochastic Structural Dynamics, Progress in Theory and Applications, Ariaratnm, S.T., Schueller, G.I. and Elishakoff, I. eds., Elsevier Applied Science, pp. 241-291.

70) Sih, G.C. 1974. Strain Energy Density Factor Applied to Mixed Mode Crack Problems. Int. J. Fracture Mech., **10**, pp.305-322.

71) Spanos, P.D. and Ghanem, R. 1988. Stochastic Finite Element Expansion for Random Media. Report NCEER-88-0005.

72) Sues, R.H., Chen, H.-C., Twisdale, L.A. 1991. Probabilistic Structural Mechanics Research for Parallel Processing Computers NASA CR-187162.

73) Sues, R.H., Chen, H.-C., Chamis, C.C., Murthy, P.L.N. 1992a. Programming probabilistic structural analysis for parallel processing computers. AIAA Journal, scheduled for publication.

74) Sues, R.H. Lua, Y.J., and Smith, M.D. 1992b. Parallel computing for probabilistic response analysis of high temperature composites. NASA CR-26576.

75) Sues, R.H. and Chen, H.-C. 1992c. The stochastic preconditional conjugate gradient method. Probabilistic Engineering Mechanics, to be published.

76) Telles, J.C.F. 1983. The Boundary Element Method Applied to Inelastic Problems, Lecture Notes in Engineering, 1, Springer-Verlag.

77) Tong, P., Pian, T.H.H. and Lasry, S.J. 1973. A Hybrid-Element Approach to Crack Problems in Plane Elasticity. Int. J. Numer. Methods Eng. 7, pp. 297-308.

78) Tvedt, L. 1983. Two Second Order Approximations to the Failure Probability. Det Norske Veritas (Norway) RDIV/20-004-83.

79) Twisdale, L.A. and Dunn, W.L. 1983. Probabilistic analysis of tornado wind risks. J. Struct. Engng **109** (2).

80) Twisdale, L.A. and Vickery, P.J. 1991. Research on thunderstorm wind design parameters. submitted for publication in the Journal of wind Engineering and Industrial Aerodynamics.

81) Vanmarcke, E. and Grigoriu, M. 1983. Stochastic Finite Element Analysis of Simple Beams. J. Eng. Mech. **109**, pp. 1203-1214.

82) Vanmarcke, E. 1984. Random Fields, Analysis and Synthesis, MIT Press, Second Printing.

83) Wu, X.F. and Li, X.M. 1989. Analysis and Modification of Fracture Criterion for Mixed-Mode Crack. Engng Fracture Mech. **34**, pp. 55-64.

84) Wu, Y.-T., Millwater, H. R. and Cruse, T. A. 1990. Advanced probabilistic structural analysis method for implicit performance functions. AIAA Journal. **28**, pp.1663-1669.

85) Yamazaki, F.M., Shinozuka, M., and Dasgupta, G. 1988. Neumann expansion for stochastic finite element analysis. Journal of Engineering Mechanics ASCE, **114** (8), pp. 1335-1354.

86) Zhang, Y. and Der Kiureghian, A. 1991. Dynamic Response Sensitivity of Inelastic Structures. Technical Report UCB/SEMM-91/06, Department of Civil Engineering, University of California at Berkeley.

Table 7-1. Problem Constants: Single Edge-Cracked Beam with an Applied Load

Parameter	Mean	Standard Deviation	Percent
Length (L)	10.0 in	0.0	0.0
Width (W)	5.0 in	0.0	0.0
Thickness (t)	1.0 in	0.0	0.0
Young's Modulus (E)	30,000.0 ksi	3,000.0	10.0
Poisson's Ratio (v)	0.30.0	0.0	
Applied Load (P)	10.0 kip	1.0 kip	10.0
Crack Length (a)	0.01 in	0.1 in	10.0
Stress Intensity Factor (κ_I)	33.452 ksi $\sqrt{in}$	0.0 ksi $\sqrt{in}$	0.0
Fracture Toughness (κ_{Ic})	43.0 ksi $\sqrt{in}$	0.0 ksi $\sqrt{in}$	0.0

Table 7-2. Numerical Performance in Brittle Fracture Reliability Analysis

Randomness in	Variance (kip^2/in^3)	Starting Point	Number Iterations	Failure Point	Reliability Index	Probability of Failure
Force	12.3248 9.94 %	P=12.5 kip	5	P=12.2 kip	2.173	1.49 %
Young's Modulus	0.003087 0.18 %	E=30e3 ksi	0	E=30e3 ksi	∞	0.0 %
Crack Length	1.8273 3.83 %	a=1.4 in	7	a=1.29 in	2.911	0.1801 %
Combined	12.5107 10.01 %	P=12 kip E=30e3 ksi a=1.1 in	9	P=12.1 kip E=30e3 ksi a=1.02 in	2.079	1.88 %

Table 7-3. Problem Constants: Single Edge-Cracked Plate with a Distributed Load

Parameter	Mean	Standard Deviation	Percent
Length (L)	10.0 in	0.0	0.0
Width (W)	4.0 in	0.0	0.0
Thickness (t)	1.0 in	0.0	0.0
Young's Modulus (E)	30,000.0 ksi	0.0	0.0
Poisson's Ratio (ν)	0.3	0.0	0.0
Applied Stress (τ)	12.0 ksi	3.0 ksi	25.0
Initial Crack Length (a_1)	0.01 in	0.01 in	100.0
Final crack Length (a_f)	0.1 in	0.01 in	10.0
Fatigue Parameter (D)	1.0×10^{-10}	3.0×10^{-11}	30.0
Fatigue Parameter (n)	3.25	0.08	2.5

Table 7-4. The Statistical Parameters and Distributions of Input Random Variables of the Example Problem

Random Parameters	Mean	Standard deviation	COV
a_i (Uniform with tail)	0.5833×10^{-2} in	0.3584×10^{-2} in	61.4%
D (Log-normal)	0.3770×10^{-9}	0.1885×10^{-10}	5.0%
n (Log-normal)	3.60	0.18	5.0%
τ (Normal)	11.0 ksi	1.1 ksi	10.0%
x_c (Uniform)	-0.25 in	0.14433	57.7%
y_c (Uniform)	-0.4 in	0.05774	14.4%
r_c (Uniform)	0.1375 in	0.03608	26.2%
p_i (Normal)	35.0 ksi	3.5	10.0%

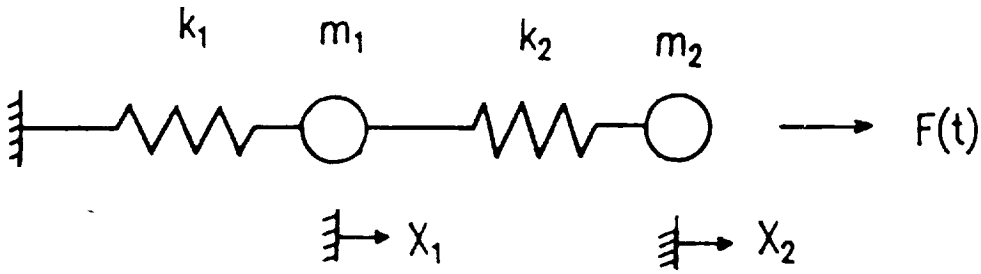

$$F(t)=25.0 \times 10^6 \sin(2000t)$$

$m_1=0.372$ $\quad k_1=24.0 \times 10^6$

$m_2=0.248$ $\quad k_2=12.0 \times 10^6$

Figure 7-1

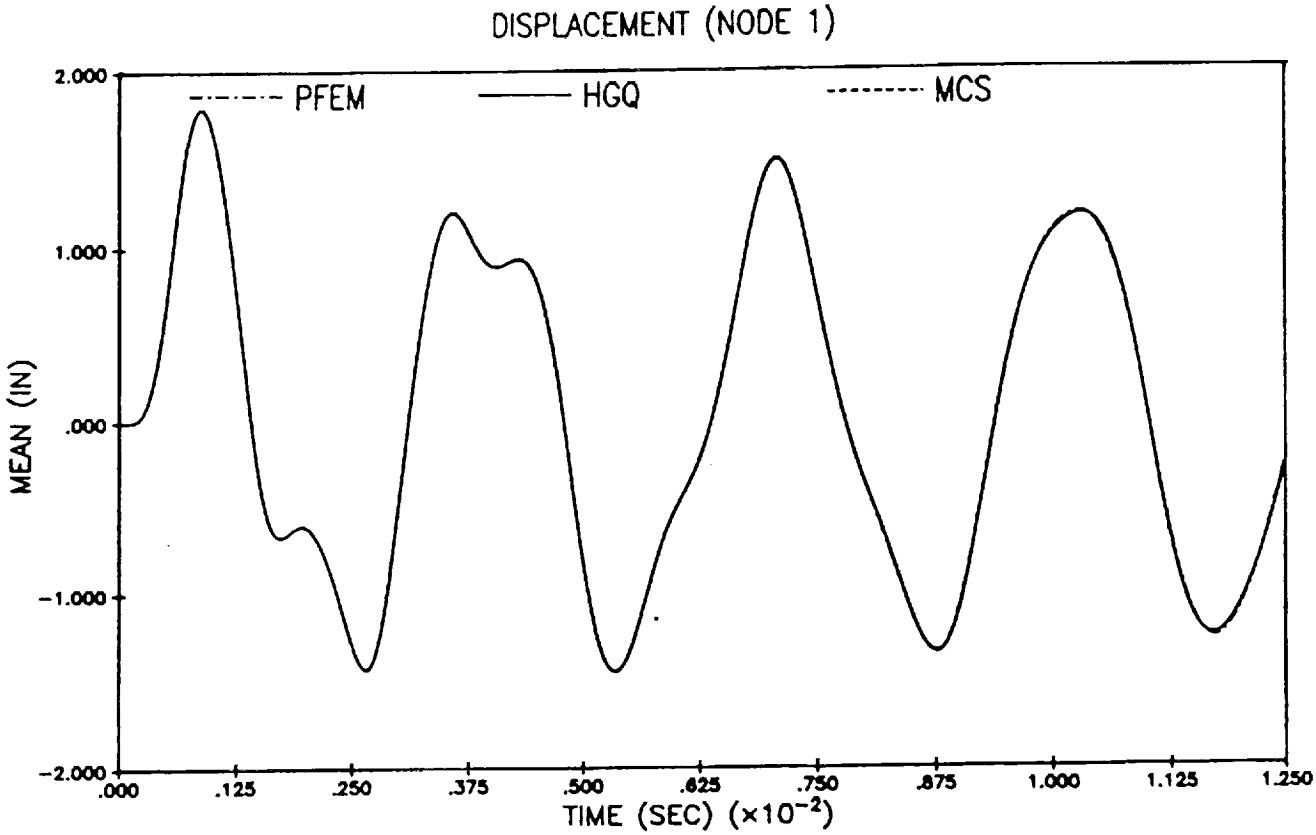
DISPLACEMENT (NODE 1)
PFEM
HGQ
MCS
2.000
1.000
.000
-1.000
-2.000
MEAN (IN)
.000
.125
.250
.375
.500
.625
.750
.875
1.000
1.125
1.250
TIME (SEC) (×10⁻²)

Figure 7-2

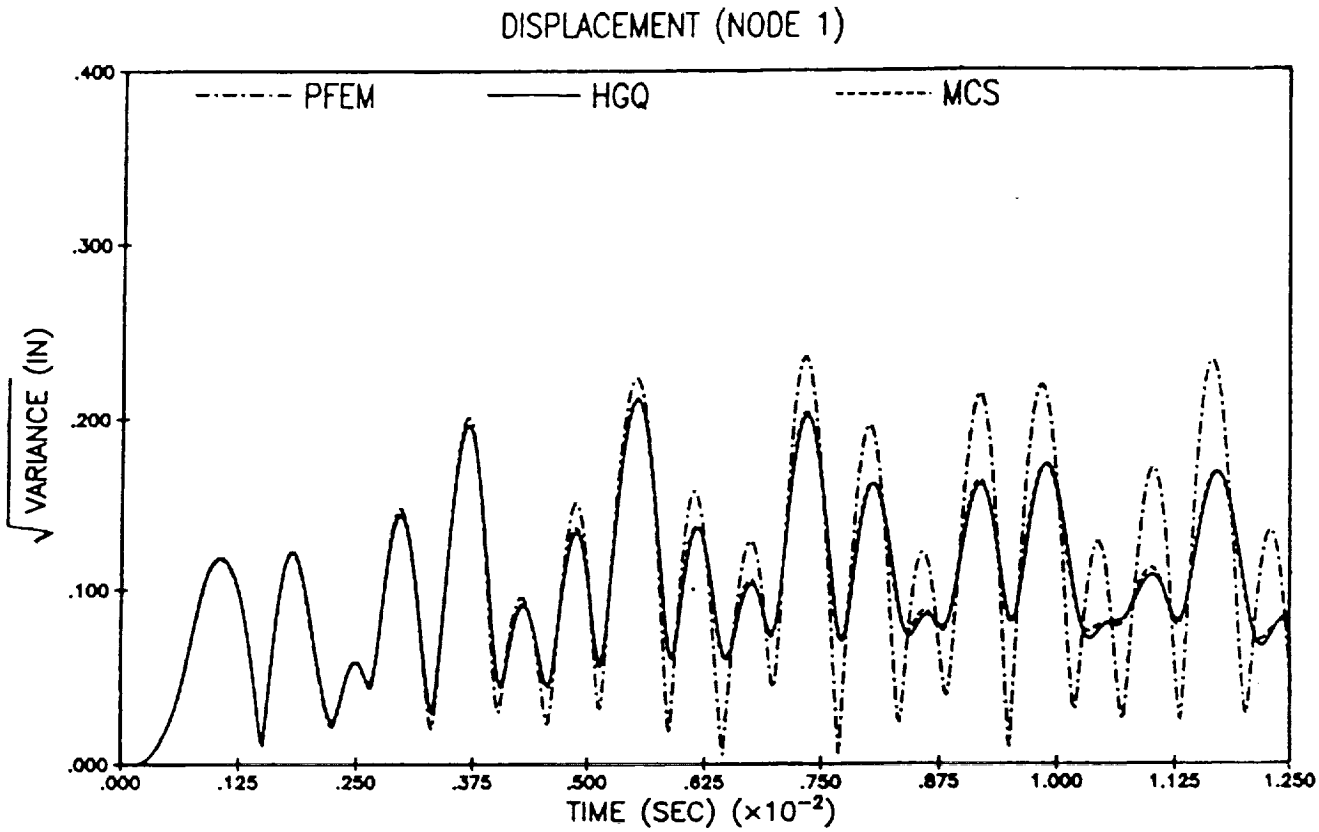
DISPLACEMENT (NODE 1)
PFEM
HGQ
MCS
√VARIANCE (IN)
.400
.300
.200
.100
.000
.000
.125
.250
.375
.500
.625
.750
.875
1.000
1.125
1.250
TIME (SEC) (×10⁻²)

Figure 7-3

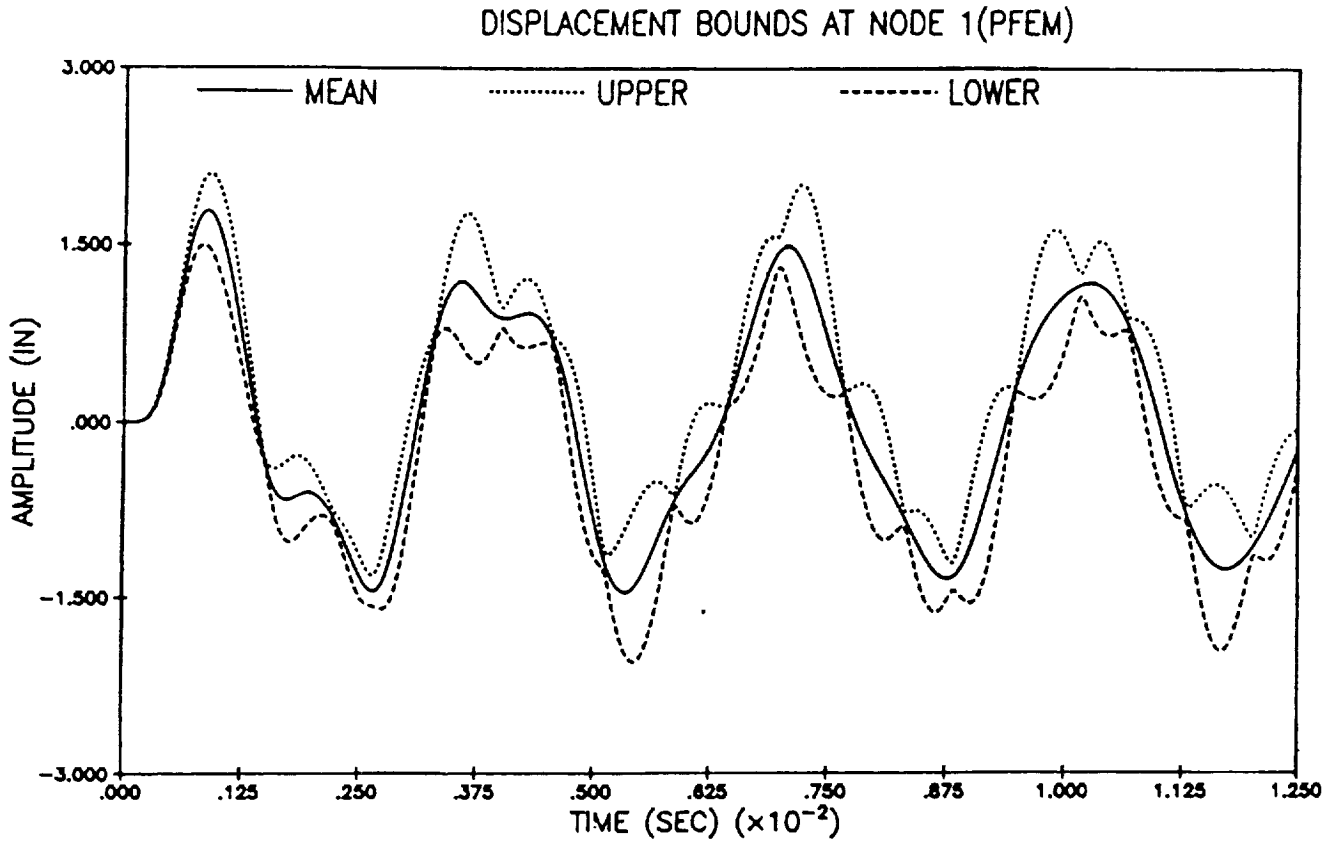
DISPLACEMENT BOUNDS AT NODE 1(PFEM)
MEAN
UPPER
LOWER
AMPLITUDE (IN)
3.000
1.500
.000
-1.500
-3.000
.000
.125
.250
.375
.500
.625
.750
.875
1.000
1.125
1.250
TIME (SEC) (×10⁻²)

Figure 7-4

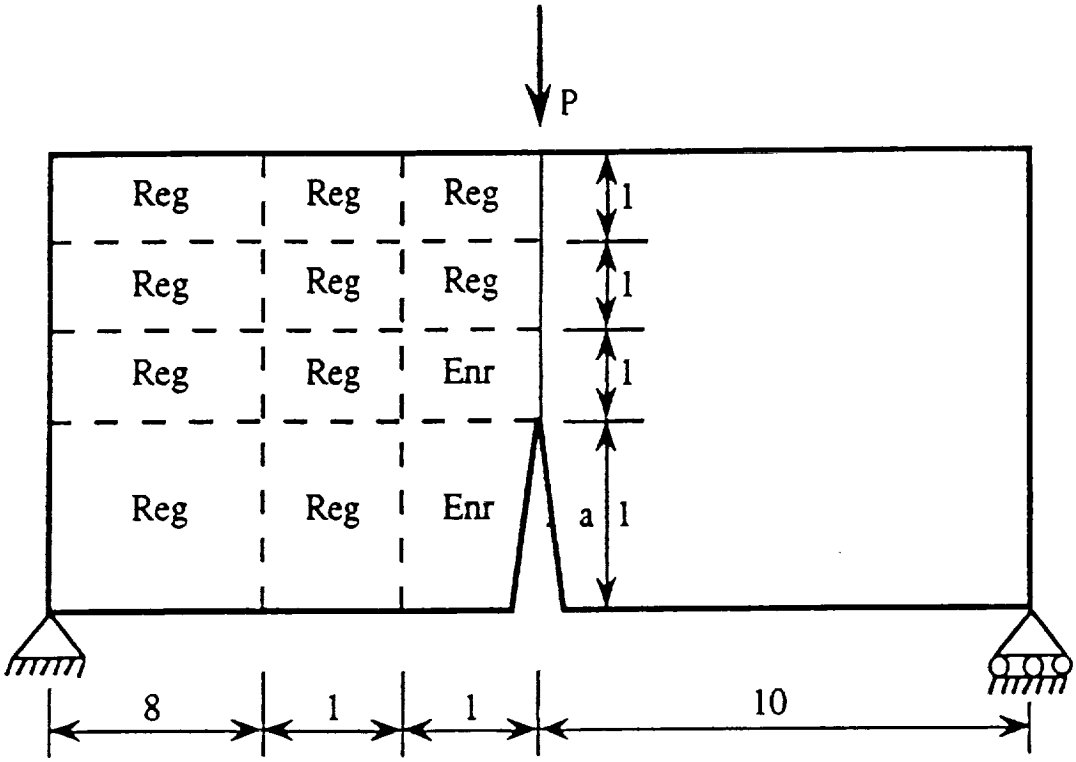
P
Reg
Reg
Reg
Reg
Reg
Reg
Reg
Reg
Reg
Reg
Reg
Enr
Reg
Reg
Enr
1
1
1
a
1
8
1
1
10

Figure 7-5

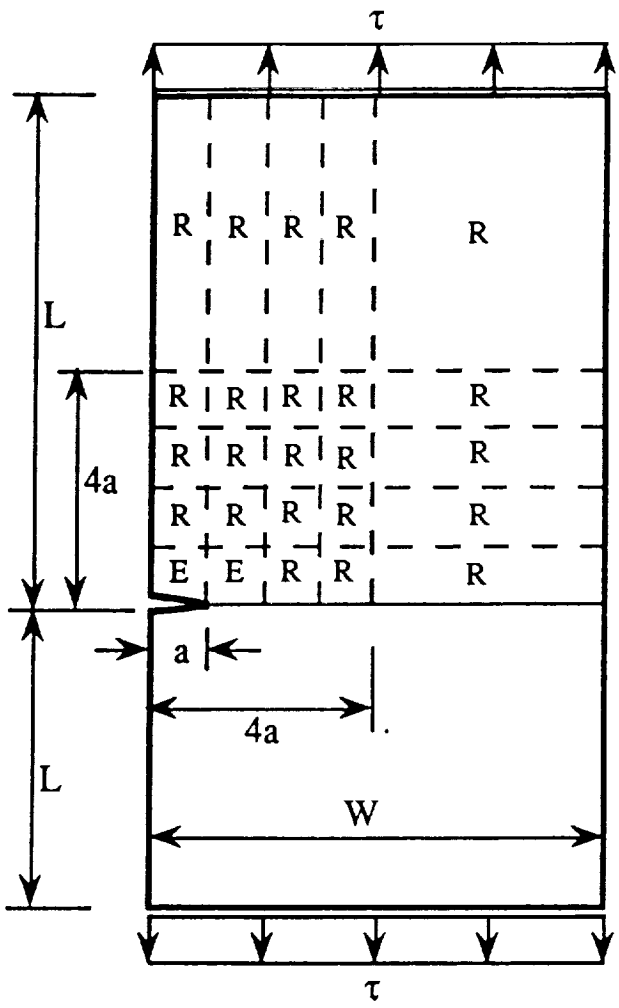

Figure 7-6

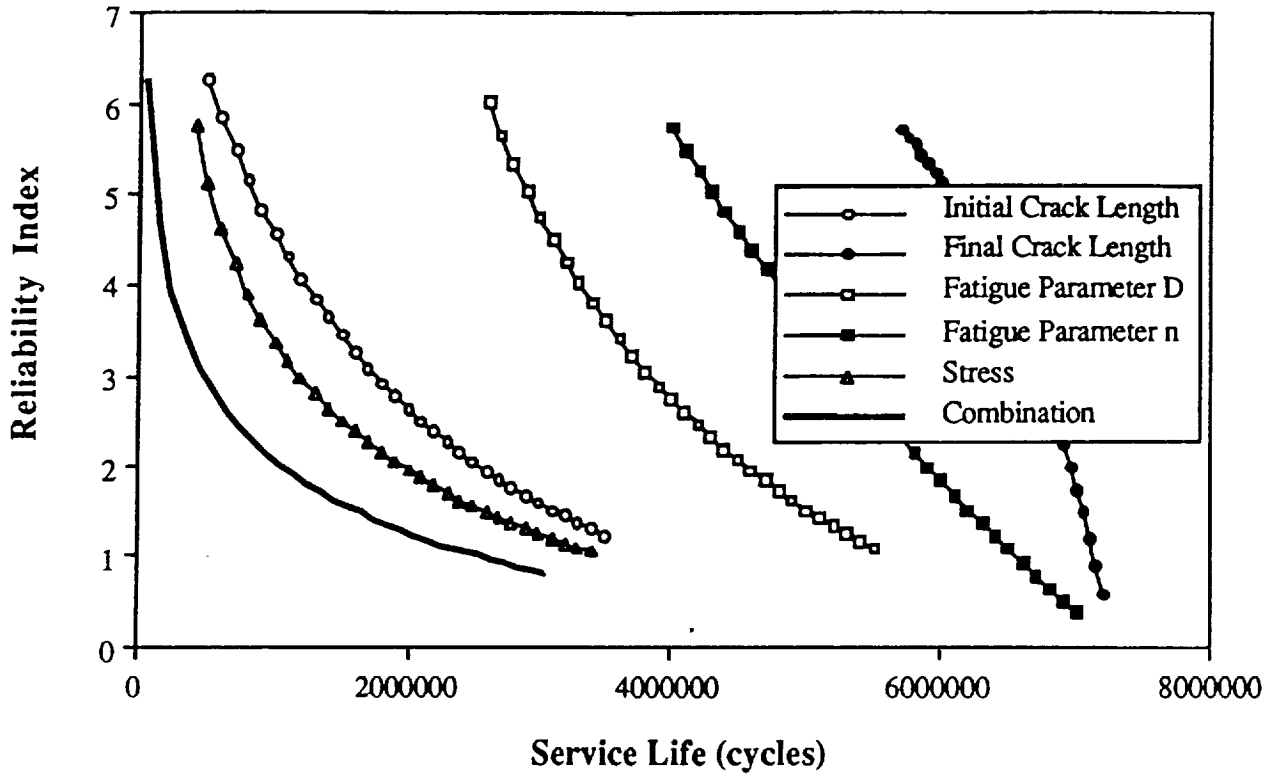
Reliability Index
Service Life (cycles)
0
1
2
3
4
5
6
7
0
2000000
4000000
6000000
8000000
Initial Crack Length
Final Crack Length
Fatigue Parameter D
Fatigue Parameter n
Stress
Combination

Figure 7-7a

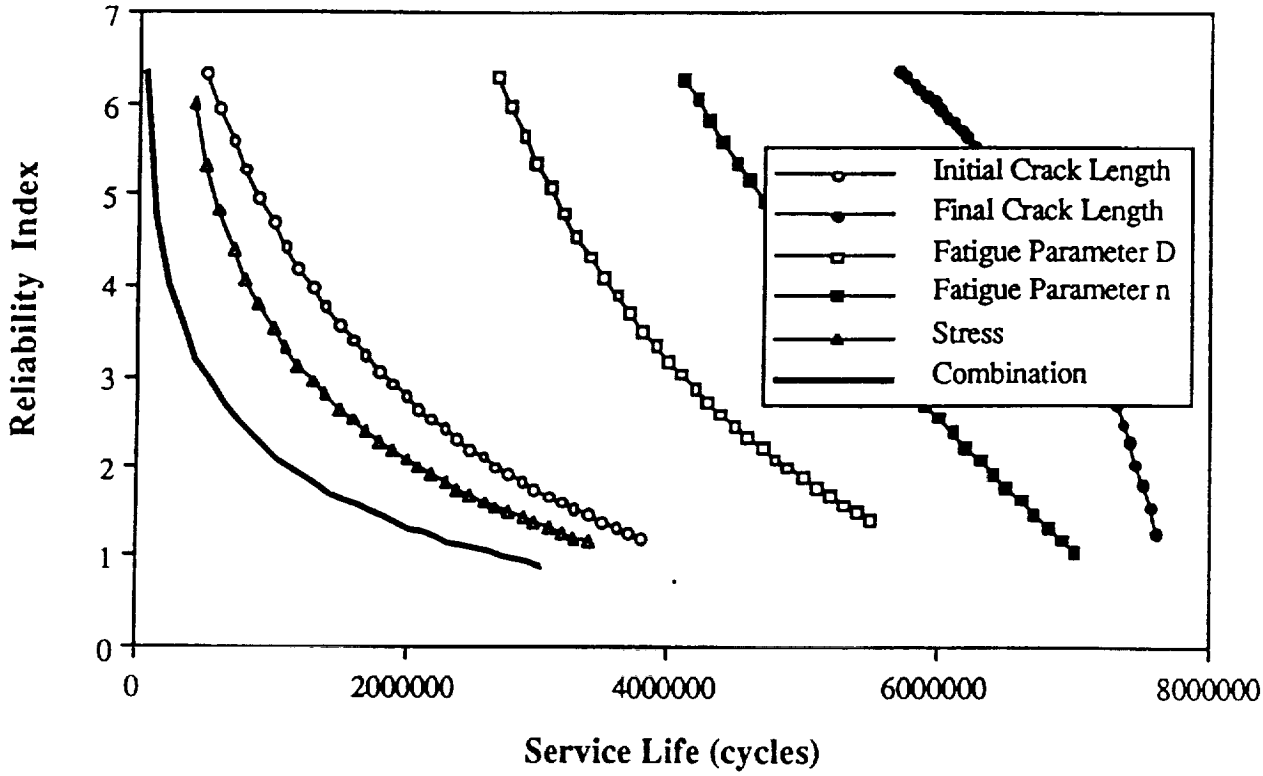
Reliability Index
7
6
5
4
3
2
1
0
0
2000000
4000000
6000000
8000000
Service Life (cycles)
Initial Crack Length
Final Crack Length
Fatigue Parameter D
Fatigue Parameter n
Stress
Combination

Figure 7-7b

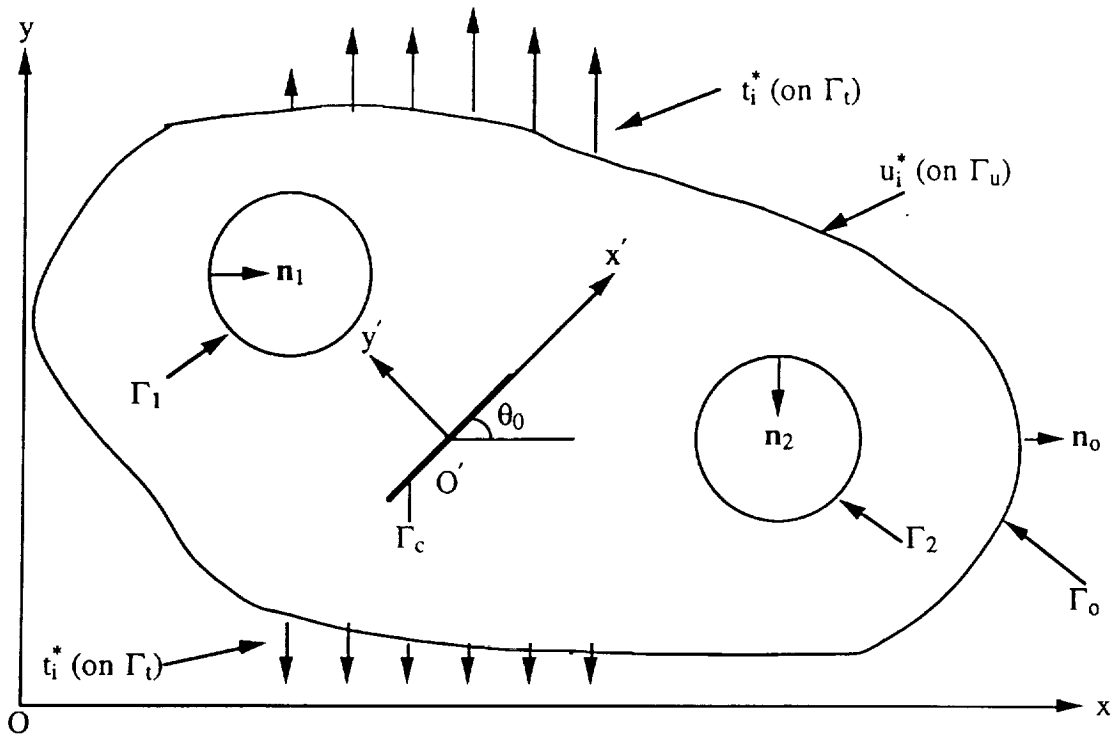
y
t_i^* (on Γ_t)
u_i^* (on Γ_u)
n_1
x′
y′
Γ_1
θ_0
O′
n_2
n_o
Γ_c
Γ_2
Γ_o
t_i^* (on Γ_t)
O
x

Figure 7-8

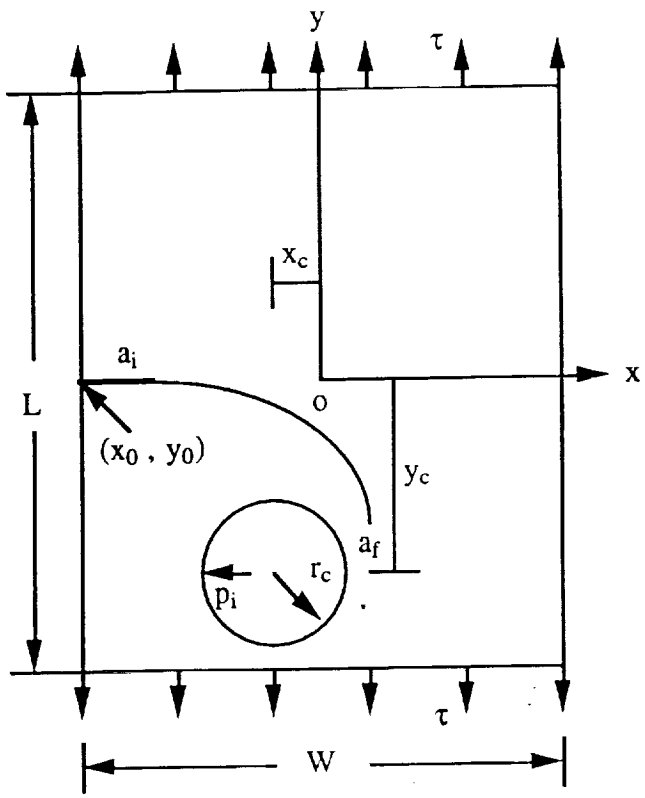

Figure 7-9

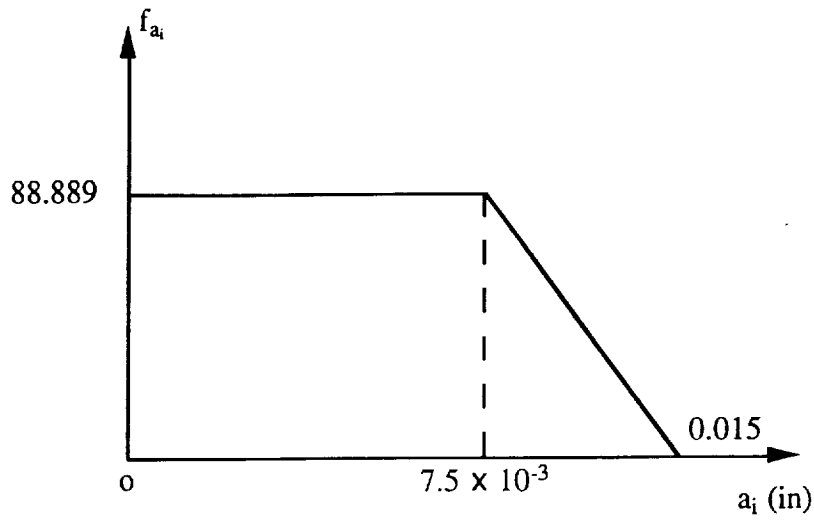

Figure 7-10

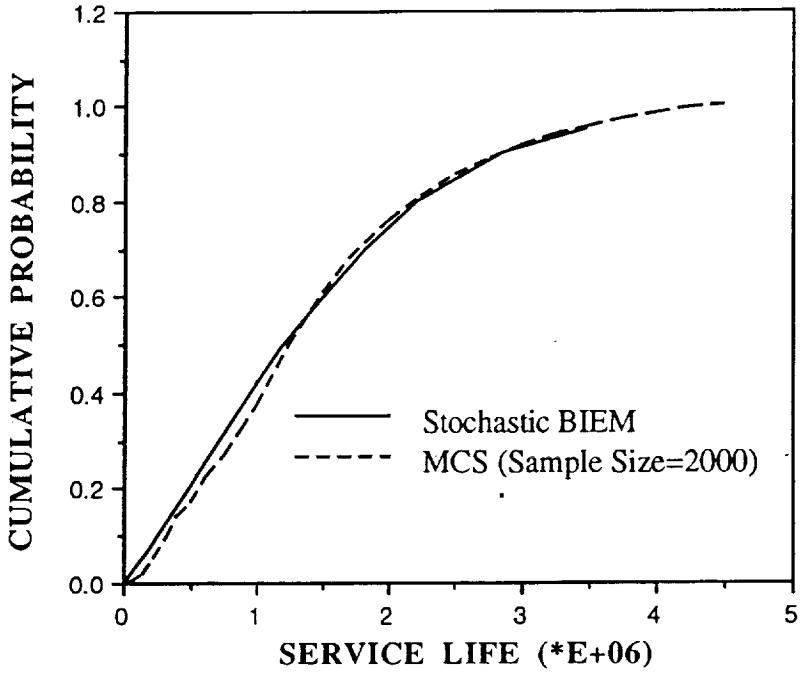
CUMULATIVE PROBABILITY
1.2
1.0
0.8
0.6
0.4
0.2
0.0
0
1
2
3
4
5
SERVICE LIFE (*E+06)
Stochastic BIEM
MCS (Sample Size=2000)

Figure 7-11

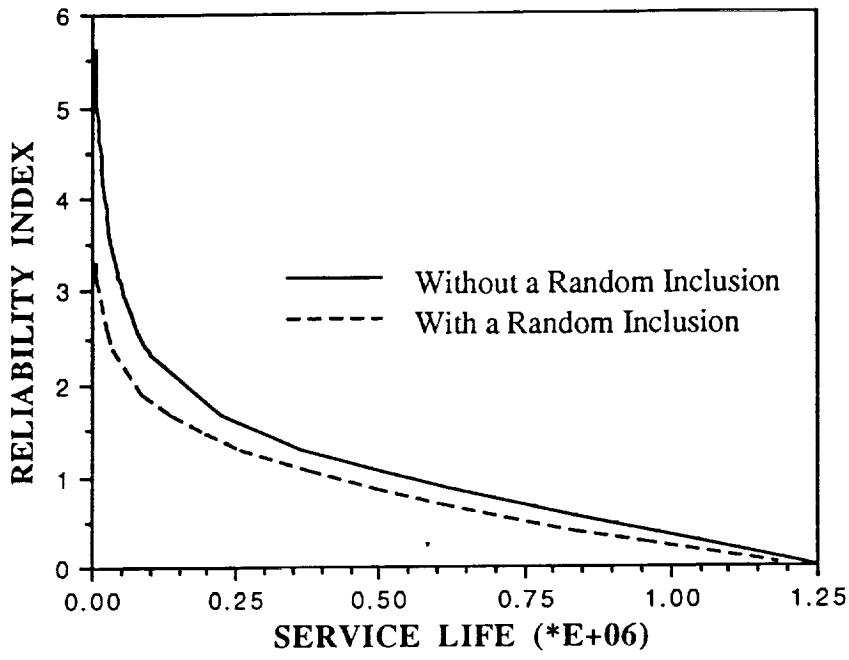
RELIABILITY INDEX
6
5
4
3
2
1
0
0.00
0.25
0.50
0.75
1.00
1.25
SERVICE LIFE (*E+06)
Without a Random Inclusion
With a Random Inclusion

Figure 7-12

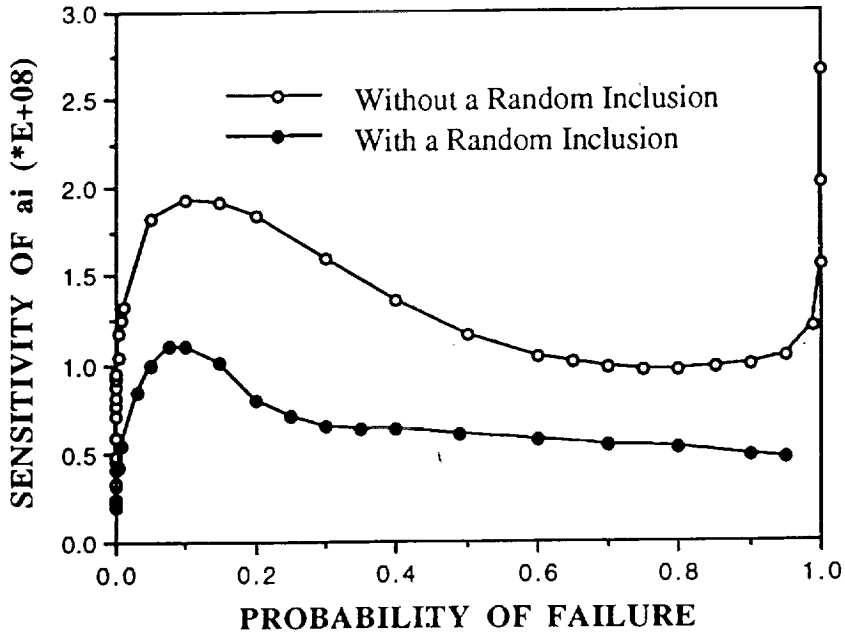
3.0
2.5
2.0
1.5
1.0
0.5
0.0
SENSITIVITY OF ai (*E+08)
Without a Random Inclusion
With a Random Inclusion
0.0
0.2
0.4
0.6
0.8
1.0
PROBABILITY OF FAILURE

Figure 7-13

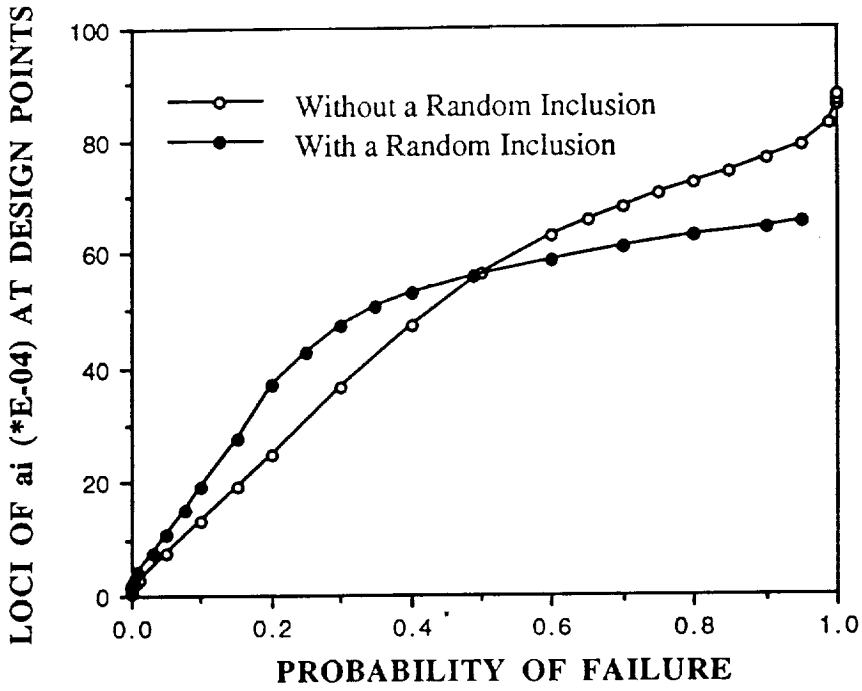
LOCI OF ai (*E-04) AT DESIGN POINTS
100
80
60
40
20
0
0.0
0.2
0.4
0.6
0.8
1.0
PROBABILITY OF FAILURE
Without a Random Inclusion
With a Random Inclusion

Figure 7-14

Figure Captions

Figure 7-1. A simple two degree of freedom spring-mass system.

Figure 7-2. Comparison of the Mean Displacement at node 1 using: a) probabilistic finite element method; b) Hermite-Gauss quadrature; c) Monte Carlo simulation.

Figure 7-3. Comparison of variance of displacement at node 1 using: a) probabilistic finite element method; b) Hermite-Gauss quadrature; c) Monte Carlo simulation.

Figure 7-4. $\pm 3\sigma$ bounds of the displacement at node 1 using probabilistic finite element method.

Figure 7-5. Problem statement: single edge-cracked beam with an applied load.

Figure 7-6. Model for single edge-cracked plate with an applied load.

Figure 7-7a. Reliability index for the reference solution showing the effects of uncertainty in the individual variables and their combined effect.

Figure 7-7b. Reliability index for the PFEM solution showing the effects of uncertainty in the individual variables and their combined effect.

Figure 8. A multi-connected elastic body containing a finite crack under remote loading.

Figure 9. A single edge-cracked plate with a random transformation inclusion subjected to a distributed load.

Figure 10. The uniform with tail distribution for the initial crack length a_i .

Figure 11. Comparison of CDF of the fatigue life T obtained by stochastic BIEM with the results of MCS for the example problem.

Figure 12. Comparison of reliability index of two cases.

Figure 13. Comparison of response sensitivity at a_i design points of two cases.

Figure 14. Comparison of the locus of a_i at design points of two cases.